

The HST Key Project on the Extragalactic Distance Scale XIV. The Cepheids in NGC 1365¹

N. A. Silbermann,² Paul Harding,³ Laura Ferrarese,⁴ Peter B. Stetson,⁵ Barry F. Madore,⁶ Robert C. Kennicutt, Jr.,³ Wendy L. Freedman,⁷ Jeremy R. Mould,⁸ Fabio Bresolin,³ Holland Ford,⁹ Brad K. Gibson,⁸ John A. Graham,¹⁰ Mingsheng Han,¹¹ John G. Hoessel,¹¹ Robert J. Hill,¹² John Huchra,¹³ Shaun M.G. Hughes,¹⁴ Garth D. Illingworth,¹⁵ Dan Kelson,¹⁵ Lucas Macri,¹³ Randy Phelps,⁷ Daya Rawson,⁸ Shoko Sakai,² and Anne Turner³

ABSTRACT

We report the detection of Cepheid variable stars in the barred spiral galaxy NGC 1365, located in the Fornax cluster, using the Hubble Space Telescope Wide Field and Planetary Camera 2. Twelve V (F555W) and four I (F814W) epochs of observation were obtained. The two photometry packages, ALLFRAME and DoPHOT, were separately used to obtain profile-fitting photometry of all the stars in the HST field. The search for Cepheid variable stars resulted in a sample of 52 variables, with periods between 14 and 60 days, in common with both datasets. ALLFRAME photometry and light curves of the Cepheids are presented. A subset of 34 Cepheids were selected on the basis of period, light curve shape, similar ALLFRAME and DoPHOT periods, color, and relative crowding, to fit the Cepheid period-luminosity relations in V and I for both ALLFRAME and DoPHOT. The measured distance modulus to NGC 1365 from the ALLFRAME photometry is 31.31 ± 0.20 (random) ± 0.18 (systematic) mag, corresponding to a distance of 18.3 ± 1.7 (random) ± 1.6 (systematic) Mpc. The reddening is measured to be $E(V-I) = 0.16 \pm 0.08$ mag. These values are in excellent agreement with those

¹Based on observations with the NASA/ESA *Hubble Space Telescope* obtained at the Space Telescope Science Institute, which is operated by AURA, Inc. under NASA Contract No. NAS5-26555.

²Infrared Processing and Analysis Center, Jet Propulsion Laboratory, California Institute of Technology, MS 100-22, Pasadena, CA 91125

³Steward Observatory, University of Arizona, Tucson, AZ 85721

⁴Hubble Fellow, California Institute of Technology, Pasadena, CA 91125

⁵Dominion Astrophysical Observatory, Victoria, British Columbia V8X 4M6 Canada

⁶NASA Extragalactic Database, Infrared Processing and Analysis Center, California Institute of Technology, MS 100-22, Pasadena, CA 91125

⁷Observatories of the Carnegie Institution of Washington, Pasadena CA 91101

⁸Mount Stromlo and Siding Spring Observatories, Institute of Advanced Studies, ANU, ACT 2611 Australia

⁹Johns Hopkins University and Space Telescope Science Institute, Baltimore, MD 21218

¹⁰Dept. of Terrestrial Magnetism, Carnegie Institution of Washington, Washington D.C. 20015

¹¹University of Wisconsin, Madison, Wisconsin 53706

¹²Laboratory for Astronomy & Solar Physics, NASA Goddard Space Flight Center, Greenbelt MD 20771

¹³Harvard Smithsonian Center for Astrophysics, Cambridge, MA 02138

¹⁴Royal Greenwich Observatory, Cambridge CB3 0EZ England

¹⁵Lick Observatory, University of California, Santa Cruz CA 95064

obtained using the DoPHOT photometry, namely a distance modulus of 31.26 ± 0.10 mag, and a reddening of 0.15 ± 0.10 mag (internal errors only).

Subject headings: galaxies: individual (NGC 1365) — galaxies: distances — stars: Cepheids

1. Introduction

The observations presented in this paper are part of the *Hubble Space Telescope* Key Project on the Extragalactic Distance Scale, a detailed description of which can be found in Kennicutt, Freedman & Mould (1995). The main goal of the Key Project is to measure the Hubble Constant, H_0 , to an accuracy of 10%, by using Cepheids to calibrate several secondary distance indicators such as the planetary nebula luminosity function, the Tully–Fisher relation, surface brightness fluctuations, and methods using supernovae. These methods will then be used to determine the distances to more distant galaxies whereby the global Hubble Constant can be measured. Published results from other Key Project galaxies include M81 (Freedman *et al.* 1994), M100 (Ferrarese *et al.* 1996), M101 (Kelson *et al.* 1996), NGC 925 (Silbermann *et al.* 1996), NGC 3351 (Graham *et al.* 1997), NGC 3621 (Rawson *et al.* 1997), NGC 2090 (Phelps *et al.* 1998), NGC 4414 (Turner *et al.* 1998), NGC 7331 (Hughes *et al.* 1998), and NGC 2541 (Ferrarese *et al.* 1998).

NGC 1365 ($\alpha_{1950} = 3^{\text{h}}31^{\text{m}}$, $\delta_{1950} = -36^{\circ}18'$) is a large, symmetric, barred spiral galaxy with a measured heliocentric velocity of 1652 km s^{-1} (Sandage & Tammann 1981) located in the Fornax cluster of galaxies. It is classified as an SBb(s)I galaxy by Sandage & Tammann and as an SBs(b) galaxy by de Vaucouleurs *et al.* (1991). Work by Veron *et al.* (1980) found that NGC 1365 contains a hidden Seyfert 1 nucleus. NGC 1365 has been extensively mapped in HI by Ondrechen & van der Hulst (1989) and more recently by Jörsäter & van Moorsel (1995). In particular, Jörsäter & van Moorsel found that the inner disk of NGC 1365 has a significantly different inclination angle (40°) compared to previous work using optical isophotes (55°) by Linblad (1978). Other inclination angles found in the literature are 56° (Bartunov *et al.* 1994), 61° (Schoniger & Sofue 1994, Aaronson *et al.* 1981), $44^{\circ} \pm 5^{\circ}$ (Bureau, Mould, & Staveley-Smith 1996), $46^{\circ} \pm 8^{\circ}$ (Ondrechen & van der Hulst 1989) and 63° (Tully 1988). This scatter is a result of the warped nature of the NGC 1365 disk (Jörsäter & van Moorsel 1995) combined with the various observational methods the authors used to determine the the major and minor axis diameters. The true inclination angle of NGC 1365 is not vital for our Cepheid work but is critical for photometric and HI line-width corrections for the Tully-Fisher (TF) relation. If one uses infrared (H band) absolute magnitudes the effect of using the various inclination angles between 40° to 63° is minimal as the extinction correction in the infrared is small. However, the correction to the line-width, $(\sin i)^{-1}$, is not small. The corrected HI line width will decrease by 40% if one uses 63° instead of 40° . Detailed discussion of the TF method is beyond the scope of this paper but we caution readers to accurately determine the inclination angle of NGC 1365 before using it as a TF calibrator.

Overall, Fornax is a relatively compact cluster of about 350 galaxies with a central, dense concentration of elliptical galaxies. The center of the cluster is dominated by the large E0 galaxy NGC 1399, with NGC 1365 lying ~ 0.5 Mpc from NGC 1399 as projected on the sky. The heliocentric radial velocity of the Fornax cluster is 1450 km s^{-1} with a dispersion of 330 km s^{-1} (Held & Mould 1994). The Fornax cluster has been the target of many studies involving secondary distance indicators, as reviewed by Bureau, Mould, & Staveley-Smith (1996). A Cepheid distance to the cluster will be an important step forward in calibrating the extragalactic distance scale.

This is the first of two papers on the Cepheid distance to NGC 1365 and the Fornax cluster. This paper describes the HST observations of Cepheid variable stars in NGC 1365 and the distance derived to the galaxy. A companion paper by Madore *et al.* (1998a) discusses the implications for the distance to the Fornax cluster and the calibration of the extragalactic distance scale. The location of NGC 1365 within the Fornax cluster and the geometry of the local universe is discussed in Madore *et al.* (1998b). We note that the Key Project has recently observed two other galaxies within the Fornax cluster, NGC 1425 (Mould *et al.* 1998) and NGC 1326A (Prosser *et al.* 1998).

2. Observations

NGC 1365 was imaged using the Hubble Space Telescope’s Wide Field and Planetary Camera 2 (WFPC2). A description of WFPC2 instrument is given in the HST WFPC2 Instrument Handbook (Burrows *et al.* 1994). The camera consists of four 800×800 pixel CCDs. Chip 1 is the Planetary Camera with 0.046 arcsec pixels and an illuminated $\sim 33 \times 31$ arcsec field of view. The three other CCDs make up the Wide Field Camera (Chips 2-4), each with 0.10 arcsec pixels and a $\sim 1.25 \times 1.25$ arcmin illuminated field of view. Each CCD has a readout noise of about $7 e^-$. A gain setting of $7 e^-/\text{ADU}$ was used for all of the NGC 1365 observations.

WFPC2 imaged the eastern part of NGC 1365, as seen in Figure 1, from 1995 August through September. As with all the galaxies chosen for the Key Project, the dates of observation were selected using a power-law time series to minimize period aliasing and maximize uniformity of phase coverage for the expected range of Cepheid periods from 10 to 60 days (Freedman *et al.* 1994). Twelve epochs in V (F555W) and four in I (F814W) were obtained. Each epoch consisted of two exposures, taken on successive orbits, with typical integration times of 2700 seconds. All observations were made with the camera at an operating temperature of -88°C . Table 1 lists the image identification code, Heliocentric Julian Date of observation (mid-exposure), exposure time, and filter, of each observation. On 1995 August 28 the focus of HST was changed, occurring between the 5th and 6th epoch of NGC 1365 observations. The effect of this refocus is discussed in Section 3.1.

3. Photometric Reductions

All observations were preprocessed through the standard Space Telescope Science Institute (STScI) pipeline as described by Holtzman *et al.* (1995b). The images were calibrated with the most up-to-date version of the routine reference files provided by the Institute at the time the images were taken. Our post-pipeline processing included masking out the vignetted edges, bad columns, and bad pixels. The images were then multiplied by a pixel area map to correct for the WFPC2 geometric distortion (Hill *et al.* 1998), multiplied by 4, and converted to integer values. Then the ALLFRAME and DoPHOT photometry packages were used to obtain profile-fitting photometry of all the stars in the HST images. Details of each method are described below.

3.1. DAOPHOT II/ALLFRAME Photometry

The extraction of stellar photometry from CCD images using the ALLFRAME (Stetson 1994) package first requires a robust list of stars in the images. The long exposures of NGC 1365 contain significant numbers of cosmic ray events which can be misidentified as stars by automated star-finding programs. To solve this problem, images for each chip were median averaged to produce a clean cosmic ray free image. DAOPHOT II and ALLSTAR (Stetson 1987, Stetson *et al.* 1990, Stetson 1991, 1992, 1994) were then used to identify the stars in the deep, cosmic ray free images for each chip. The star lists were subsequently used by ALLFRAME to obtain profile-fitting photometry of the stars in the original images. The point spread functions were derived from public domain HST WFPC2 observations of the globular clusters Pal 4, and NGC 2419.

Ten to twenty fairly isolated stars in each WFPC2 chip were chosen to correct the profile-fitting ALLFRAME photometry out to the 0.5 arcsec system of Holtzman *et al.* (1995a). These stars are listed in the appendix as secondary standards to our photometric reductions. To remove the effects of nearby neighbors on the aperture photometry all the other stars were first subtracted from the images. Growth curves for the isolated stars were constructed using DAOGROW (Stetson 1990). Best estimates of the aperture corrections were determined by running the program COLLECT (Stetson 1993), which uses the profile-fitting photometry and the growth-curve photometry to determine the best photometric correction out to the largest aperture, 0.5 arcsec in our case.

As with the previous Key Project galaxy NGC 925 (Silbermann *et al.* 1996), the aperture corrections (ACs) for all the frames in each filter were averaged to produce mean ACs that were then applied to each frame to shift the Cepheid photometry onto the Holtzman *et al.* 0.5 arcsec system. For nonvariable stars, mean instrumental V and I magnitudes averaged over all epochs were calculated using DAOMASTER (Stetson 1993) and then shifted to the 0.5 arcsec system using the mean ACs. However, for NGC 1365 we noticed there were relatively large variations in the individual frame ACs, typically on the order of ± 0.07 mag, but for one case as large as -0.2 mag, from the mean values. These variations are due to random photometric scatter in the small number of isolated, bright stars available to us for AC determination, and the realization that on any given image, a few of these stars may be corrupted by comic ray events or chip defects further reducing the number of usable AC stars for a particular image. There was also a focus change between the 5th and 6th epoch, which resulted in an obvious shift of about $+0.1$ mag in the individual ACs for epochs obtained after the focus change. As a result, we also calculated mean magnitudes and fit period-luminosity relations for the Cepheids using photometry corrected by individual frame ACs. The typical difference between mean V and I magnitudes for the Cepheids (mean ACs – individual ACs) was $+0.01$ mag, and for some of the Cepheids was as large as $+0.02$ mag. Due to the refocusing event and the relatively large variation in the individual ACs we feel that the individual photometric measurements of the Cepheids at each epoch are best represented using the individual ACs. The effect on the distance modulus to NGC 1365 is minimal, $+0.01$ mag. Throughout the rest of this paper we will use the individual AC corrected Cepheid photometry.

The final form of the conversion equations for the ALLFRAME photometry is:

$$M = m + 2.5 \log t - C_1(V - I) + C_2(V - I)^2 + AC + ZP \quad (1)$$

where M the standard magnitude, m is the instrumental magnitude, t is the exposure time, C_1 and C_2 are the color coefficients, AC is the aperture correction (different for each frame for the Cepheids), and ZP is

the zero point. Since we have shifted our photometry to the 0.5 arcsec system of Holtzman *et al.* (1995a) we use their color coefficients from their Table 7: $C_1 = -0.052$ for V and -0.063 for I , and $C_2 = 0.027$ for V and 0.025 for I . The ZP term includes the Hill *et al.* (1998) long exposure zero point, the ALLFRAME zero point of -25.0 mag, and a correction for multiplying the images by four before converting them to integers ($2.5\log(4.0)$). For V band the ZP terms are -0.984 ± 0.02 , -0.973 ± 0.01 , -0.965 ± 0.01 , and -0.989 ± 0.02 for Chips 1–4 respectively, and for I band are -1.879 ± 0.04 , -1.838 ± 0.02 , -1.857 ± 0.02 , and -1.886 ± 0.01 for Chips 1–4 respectively. For each epoch, an initial guess of each star’s color, $V - I = 0.0$, was used and the V and I equations were then solved iteratively.

For the nonvariable stars, an average magnitude over all epochs was calculated using DAOMASTER, which corrects for frame-by-frame differences due to varying exposure times and focus, and the equations above were used to calculate the final standard V and I magnitudes using mean aperture corrections for each chip and filter combination.

3.2. DoPHOT Photometry

As a double-blind check on our reduction procedures, we separately reduced the NGC 1365 data using a variation of DoPHOT (Schechter *et al.* 1993) described by Saha *et al.* (1996). The DoPHOT reductions followed the procedure described by Saha *et al.*, Ferrarese *et al.* (1996) and Silbermann *et al.* (1996). Here we only mention aspects of the reductions that were unique to NGC 1365. The DoPHOT reduction procedure identifies cosmic rays when combining the single epoch exposures, prior to running DoPHOT (Saha *et al.* 1994). Due to the unusually long exposure times in the NGC 1365 images, however, the number of pixels affected by cosmic rays was so large that significant numbers of residual cosmic ray artifacts remained in the combined images. To overcome this problem, the combined images for each epoch were further combined in pairs, to create a single clean master image. The master image was then compared with each original image to identify and flag the cosmic rays. The process was then repeated, but with the pixels affected by cosmic ray events in both single epoch image pairs flagged. This process was iterated several times to ensure both a clean master image, and that tips of bright stars were not incorrectly identified as cosmic rays and removed. These master images were then used to generate a coordinate list for the DoPHOT photometry.

Calibration of the DoPHOT photometry was carried out as follows. Aperture corrections were determined from the NGC 1365 frames and applied to the raw magnitudes. The magnitudes were then corrected to an exposure time of 1 second, and a zero point calibration was applied to bring them to the 0.5 arcsec system of Holtzman *et al.* (1995a). These zero point corrections are as given in Holtzman *et al.*, but with a small correction applied to account for differences in star and sky apertures (Hill *et al.* 1998). The prescription of Holtzman *et al.* was then used to convert the instrumental magnitudes to standard Johnson V and Cousins I magnitudes.

3.3. Comparison of DAOPHOT and DoPHOT Photometric Systems

The independent data reductions using ALLFRAME and DoPHOT provide a robust external test for the accuracy of the profile-fitting photometry of these crowded fields. Figure 2 shows the comparison between the DoPHOT and ALLFRAME final photometry. As expected we see increased scatter as one goes to fainter magnitudes. We also see that for some of the filter and chip combinations (i.e. Chip 1 V and

I bands, and Chip 2 V band) there are small scale errors, on the order of $0.01 \text{ mag mag}^{-1}$. The nature of these scale errors is still not completely clear at this time, but it is most likely due to small differences in the sky determination, which translate into correlations between the photometric error and the star magnitudes. Artificial star simulations (discussed below) show that DoPHOT is somewhat more robust than ALLFRAME in separating close companions, which will therefore be measured brighter by ALLFRAME than DoPHOT. This explains the larger number of outliers found with positive DoPHOT–ALLFRAME residuals for some filter/chip combinations.

The horizontal line in each panel in Figure 2 marks the average difference between DoPHOT and ALLFRAME, using stars brighter than 25 mag and removing wildly discrepant stars. The differences are listed in Table 2. The errors are the rms of the means. In general the differences are on the order of $\pm 0.1 \text{ mag}$, which is slightly larger than DoPHOT/ALLFRAME comparisons for other Key Project galaxies ($\sim 0.07 \text{ mag}$ or less for M101, NGC 925, NGC 3351, NGC 2090, and NGC 3621). An extensive set of simulations was carried out adding artificial stars to the NGC 1365 frames, with the intent of understanding the nature of the observed differences. The main result of these observations, discussed in detail in a subsequent paper (Ferrarese *et al.* 1998b), is that the dominant cause of uncertainty lies in the aperture corrections, while errors in sky determinations and ability to resolve close companions play only a second order role. The paucity of bright isolated stars in crowded fields makes the determination of aperture corrections problematic at best. As an extreme example, the ALLFRAME aperture corrections derived for the first and second exposure of the first I epoch differ by 0.3 mag for the PC. Since focus/jitter changes between consecutive orbit exposures are irrelevant, 0.3 mag can be taken as a reasonable estimate of the uncertainty in the aperture corrections for that particular chip/filter/epoch combination (more typical variations in the aperture corrections are $\pm 0.07 \text{ mag}$ for both the DoPHOT and ALLFRAME datasets). Similar considerations hold for the DoPHOT aperture corrections. The DoPHOT–ALLFRAME differences observed for the bright NGC 1365 stars are therefore found to be not significant when compared to the uncertainty in the aperture corrections, and simply reflect the limit to which photometric reduction can be pushed in these rather extreme fields.

We made a similar DoPHOT-ALLFRAME comparison for the 34 Cepheids used to fit the period-luminosity relations (see Section 6). The results of those comparisons are shown in Figure 3, and listed at the bottom of Table 2. The DoPHOT-ALLFRAME differences for the Cepheids show more scatter, as expected, since they are $\sim 2 \text{ mag}$ fainter than the brighter nonvariable stars in Figure 2, but overall, the Cepheids mirror the nonvariable star DoPHOT-ALLFRAME differences.

4. Identification of Variable Stars

Two methods were used to search for variable stars using the ALLFRAME dataset. In both cases, the search for variables was done using only the V photometry. The I photometry was used to help confirm variability and to determine $V - I$ colors. The first method was a search for stars with unusually high dispersion in their mean V magnitudes. A few candidate variables were found this way. The more fruitful method employed a variation on the correlated variability test suggested by Welch & Stetson (1993). First, the average magnitude and standard deviation over all epochs was calculated for each star. Any magnitude more than 2 standard deviations from the average was discarded. This removed many of the cosmic ray events. As another filter, if the magnitude difference between two single epoch observations was greater than 2.75 mag the epoch was thrown out. Note that cosmic ray events that lead to reasonably measured magnitudes (i.e. about the same as the average magnitude) slip through these filters. For each pair of

observations in an epoch, the difference between each observation and the average magnitude is then calculated. The two differences are multiplied together and summed over all epochs. The net result is that true variables will consistently have both single epoch observations brighter or fainter than the average magnitude, increasing the sum over all epochs. Random high or low observations will tend to scatter around the average but not systematically within a single epoch, so nonvariable stars will have lower sum values. Typical values of the sum were ≥ 1.0 for the variable candidates while the nonvariable stars scattered around ≤ 0.2 , with increased scatter as one went to the faintest magnitudes. Note that we discarded bad data only to derive a variability index.

After obtaining a set of variable candidates from the above procedure, the photometry for each candidate was plotted against date of observation. We were then able to note an approximate period for the candidate as well as any observations affected by cosmic-ray events. At the faint end, where we expected more contamination by nonvariable stars, we were able to exclude obvious nonvariables immediately. For candidate variables that passed this stage, any cosmic-ray event or otherwise corrupted observations were removed in anticipation of determining a period of variation. Periods for the candidate variables were found using a phase-dispersion minimization routine as described by Stellingwerf (1978). The resulting light curves were checked by eye to verify the best period for each candidate. Errors on the periods were determined by examining changes in the light curve as various periods were used. When the light curve became visibly degraded (i.e. photometry points out of phase) an upper/lower limit to the period could safely be assigned. These errors are subjective but provide the reader with a guide to how well the light curves are sampled. As a final step, the local environment of each candidate was inspected to check for severe crowding.

The search for variables in the DoPHOT reductions followed closely the procedure described in Saha & Hoessel (1990) and in Ferrarese *et al.* (1996). Candidates that were classed as having a $\geq 99\%$ confidence of being variables (based on a reduced chi-squared test) were then checked for periodicity using a variant of the method of Lafler & Kinman (1965). The number of spurious variables was minimized by requiring that the reduced chi-squared statistic be greater than 2.0 when the minimum and maximum values were removed from the calculation. The light curves of each variable candidate were then inspected individually and any alternate minima in the phase dispersion relation were checked to see which produced the best Cepheid light curve. Generally the minimum in the phase dispersion plot produced the best light curve. The image of each Cepheid candidate was also inspected at a number of epochs. Those falling in severely crowded regions or in areas dominated by CCD defects were also excluded.

The two lists of candidate variables, one from the ALLFRAME photometry and one from the DoPHOT photometry, were then compared. Any candidates found in only one dataset were located in the other dataset and checked for variability. Candidates that appeared to be real variables in *both* the ALLFRAME and DoPHOT datasets make up our final sample of 52 Cepheids in NGC 1365. Finder charts for the 52 Cepheids are shown in Figures 4 and 5. The Cepheid astrometry, periods, and period errors are given in Table 3. The variables have been labeled V1 through V52 in order of descending period. Column 1 in Table 3 identifies the Cepheids. Column 2 lists the CCD chip the Cepheid is on. Chip 1 is the Planetary Camera and Chips 2-4 are the Wide Field Camera chips. Columns 3 and 4 list the pixel position of each Cepheid, as found on image u2s70202t (see Table 1). Columns 5 and 6 give the right ascension and declination in J2000 coordinates for each Cepheid. Column 7 lists the Cepheid period in days. Column 8 gives the period error in days and column 9 lists the logarithm of the period. In addition to these 52 variables, there are several stars that appear to be definitely variable but for one reason or another did not make it into our list of definite Cepheids. Reasons include uncertain periods, questionable environment (very crowded) or

variability seen in either the ALLFRAME or DoPHOT dataset but not both. Positions, mean V and I magnitudes, and possible periods for these stars are given in Table A2 of the appendix.

5. Variable Light Curves and Parameters

To construct the ALLFRAME light curves, magnitudes obtained from images taken within a single epoch were averaged, with the resulting mean magnitude then plotted. Light curves for the Cepheids are shown in Figure 6 and the ALLFRAME photometry is listed in Tables 4 and 5. The error bars in Figure 6 are averages of the two single exposure errors as reported by ALLFRAME that make up each epoch. In cases where one of the two single exposure magnitudes is bad (i.e. cosmic ray event), the magnitude and error are from the surviving measurement. As with previous Key Project galaxies, ALLFRAME overestimates the error for a given photometric measurement in these undersampled WFPC2 images. This effect is discussed in the analysis of WFPC2 data from M101 by Stetson *et al.* (1998a). Briefly, when we compare photometric measurements within a given epoch for NGC 1365 we find that the difference between them is significantly less than the errors quoted by ALLFRAME. Typical real photometric differences are ± 0.06 mag, at the magnitude level of the Cepheids, for both V and I , while ALLFRAME reports errors significantly larger than ± 0.10 mag.

Mean V magnitudes for the Cepheids were determined two different ways. First, as in other papers in this series, since the observations were preselected to evenly sample a typical 10–60 day Cepheid light curve (Freedman *et al.* 1994), unweighted intensity averaged mean magnitudes were calculated. Second, phase-weighted mean intensity magnitudes $\langle m \rangle$ were also calculated using

$$\langle m \rangle = -2.5 \log \left[\sum_i^N 0.5(\phi_{i+1} - \phi_{i-1}) 10^{-0.4m_i} \right] \quad (2)$$

where ϕ is the phase, and the sum is over the entire light cycle. The average difference between the unweighted and phase-weighted intensity averaged mean V magnitudes is only -0.027 ± 0.002 mag for the 52 Cepheids. This difference is quite small, as expected, since most of the Cepheids have nearly uniformly sampled light curves.

With only four I observations, total mean I magnitudes were calculated as follows. Using the V and I magnitudes at the four I epochs, average V and average I magnitudes were calculated. Then, the difference between the four-epoch V average ($\langle V \rangle_4$) and 12-epoch V mean magnitude ($\langle V \rangle_{12}$) was calculated for each Cepheid. Since the amplitude of Cepheids in V is almost exactly twice the amplitude in I ($V:I = 1.00:0.51$, Freedman 1988), the four-epoch I magnitude was corrected to obtain the full 12-epoch I magnitude, as follows:

$$\langle I \rangle_{12} = \langle I \rangle_4 + 0.51(\langle V \rangle_{12} - \langle V \rangle_4). \quad (3)$$

Cosmic-ray corrupted data were removed before determining mean magnitudes. Figure 7 shows the I vs $(V - I)$ color-magnitude diagram for the HST field of NGC 1365, highlighting the 52 Cepheids. The Cepheids fall neatly between the well-defined blue plume and weak red plume of supergiants.

Table 6 lists derived ALLFRAME photometric parameters for the Cepheids. Column 1 identifies the Cepheids. Columns 2-5 list the intensity-average and phase-weighted mean V magnitudes and errors.

Columns 6-9 list the intensity-average and phase-weighted mean I magnitudes and errors. All of the errors listed in Table 6 are mean magnitude dispersions. They reflect the uncertainty due to the star’s variability (the amplitude of variation) and are not derived from the overestimated ALLFRAME errors. Column 10 and 11 lists the intensity-averaged and phase-weighted $V - I$ color of each Cepheid. A symbol in column 12 indicates the Cepheid was used in the Cepheid period-luminosity relation fit to determine the distance to NGC 1365 based on the criteria listed in the next section.

6. Period-Luminosity Relations and the Distance to NGC 1365

Standard period-luminosity (PL) relations for the LMC Cepheids are adopted from Madore & Freedman (1991) which assume a true LMC distance modulus of 18.50 mag and total line-of-sight LMC Cepheid reddening of $E(B - V) = 0.10$ mag:

$$M_V = -2.76 \log P - 1.40 \quad \text{and} \quad M_I = -3.06 \log P - 1.81. \quad (4)$$

To determine the distance to NGC 1365 a subset of the 52 Cepheids were chosen based on the following criteria. The period of the Cepheid had to be between 10 and 47 days. The lower limit of 10 days is common for all of the Key Project galaxies and was chosen to avoid first overtone pulsators which have periods less than ~ 10 days (Madore & Freedman 1991). The longest period of 47 days was estimated from our observing window of 49 days and our actual sequence of observations throughout that window. None of our Cepheids have periods under 10 days but 5 Cepheids have periods > 47 days, so they are excluded from the fit. Each variable also had to have a Cepheid-like light curve and the same period, to within 10%, in the ALLFRAME and DoPHOT datasets. Next, to exclude Cepheids that were too crowded, each Cepheid had to contribute more than 50% of the light within a 2 pixel box surrounding it. Our last criterion was that each Cepheid had to have a typical Cepheid-like color, $0.5 \leq V - I \leq 1.5$. There are a total of 34 Cepheids that satisfied all of the above criteria and they are indicated in column 11 of Table 6. These 34 Cepheids were used to fit the PL relations and determine the distance to NGC 1365.

In order to avoid incompleteness bias in fitting a slope to the NGC 1365 data, only the zero point of the regression was fitted, with the slope of the fit fixed to the LMC values. The phase-weighted V and I PL relations are shown in Figure 8. The filled circles are the 34 Cepheids used to fit the PL relations, while the open circles are the other Cepheids. The solid line in each figure represents the best fit to each dataset. The dashed lines drawn at ± 0.54 mag for the V PL relation and ± 0.36 mag for the I PL relation represent 2-sigma deviations from the mean PL relations. In the absence of significant differential reddening the intrinsic width of the Cepheid instability strip is expected to place the NGC 1365 Cepheids within these limits. We note that the full sample of 52 Cepheids are well contained within the V and I instability strips in Figure 8. From the PL fits, the apparent distance moduli to NGC 1365 are $\mu_V = 31.70 \pm 0.05$ mag and $\mu_I = 31.54 \pm 0.06$ mag, where the errors are calculated from the observed scatter in the NGC 1365 PL data themselves, appropriately reduced by the sample size of Cepheids.

The observed difference in the apparent distance moduli for NGC 1365 gives $\mu_V - \mu_I = E(V-I) = 0.16 \pm 0.08$ mag. The Key Project has adopted a reddening law of $R_V = A_V/E(V - I) = 2.45$ which is consistent with the work of Dean, Warren & Cousins (1978), Cardelli *et al.* (1989) and Stanek (1996). We therefore obtain $A_V = 0.40$ for this region of NGC 1365. The true distance modulus to NGC 1365 is then 31.31 ± 0.08 mag, corresponding to a linear distance of 18.3 ± 0.7 Mpc (internal errors only). To test how robust our calculated distance to NGC 1365 was, we also calculated the distance modulus using intensity

averaged mean magnitudes for the 34 Cepheids. The resulting true distance modulus, 31.34 mag, is just slightly larger than our result using phase-weighted mean magnitudes. As another test we used the full compliment of 52 Cepheids to fit the PL relations, using phase-weighted mean magnitudes, and obtained a distance modulus of 31.35 mag. As expected we do see a slight variation in the distance modulus depending on which mean magnitudes are used or the sample size of Cepheids but the net result is that all of these values are contained within our 31.31 ± 0.08 mag distance modulus and error.

The distance to NGC 1365 was derived independently using the Cepheid parameters derived from the DoPHOT reductions. The resulting apparent distance moduli are $\mu_V = 31.64 \pm 0.07$ mag and $\mu_I = 31.49 \pm 0.07$ mag, with a true modulus $\mu_0 = 31.26 \pm 0.10$ mag. These differ from the ALLFRAME moduli by -0.06 , -0.05 , and -0.05 mag, respectively. Despite the differences in DoPHOT and ALLFRAME photometry (Figures 2 and 3) the true distance moduli agree very well. To better understand why this is so we fit PL relations separately for each WFPC2 chip, as seen in Table 7. The scatter in individual chip apparent distance moduli is quite small for the ALLFRAME photometry and somewhat more scattered for the DoPHOT photometry. Also, DoPHOT consistently measures a smaller reddening compared to ALLFRAME for each chip and filter, except for Chip 2. Since over one-third of the Cepheids used to fit the PL relations are in Chip 2, this reduces the overall discrepancy in reddening when combining the Cepheids in all four chips. As a test, we fit PL relations excluding the Chip 2 Cepheids. The resulting true distance moduli are then 31.31 mag (no change) for ALLFRAME and 31.37 mag (change of $+0.11$ mag) for DoPHOT. The net effect of this comparison is that the ALLFRAME and DoPHOT true distance moduli still agree within their errors. Table 7 summarizes all of these PL fit tests. Column 1 in Table 7 indicates if the dataset used was the phase-weighted or intensity averaged mean V and I magnitudes. Column 2 lists which chip subset was used (1,2,3 or 4) or all 4 chips (1-4). Column 3 gives the number of Cepheids used in the fit. Columns 4 and 5 give the apparent distance moduli. Column 6 gives the extinction in magnitudes. Column 7 lists the true distance moduli for each PL fit test. The ALLFRAME results are on top, and the corresponding DoPHOT results are at the bottom.

To check for any effects due to incompleteness at the faintest magnitudes we split the final sample of 34 Cepheids into two sets of 17 Cepheids, a bright and a faint sample, sorted using the V phase-weighted ALLFRAME photometry. The true distance modulus is 31.36 ± 0.11 mag for the bright sample and 31.28 ± 0.12 mag for the faint sample. The slight changes in distance moduli seen by excluding the brightest or faintest Cepheids are not significant compared to the errors and we conclude that we are not affected by incompleteness at the faintest magnitudes.

6.1. Error Budget

Table 8 presents the error budget for the distance to NGC 1365. The errors are classified as either random or systematic based on how we will use NGC 1365 to determine the Hubble Constant. For example, the LMC distance modulus uncertainty and PL relation zero point uncertainties are systematic errors because the Key Project is using the same LMC distance modulus and Cepheid PL relation slopes for all of our galaxies. We now discuss each source of error in Table 8 in detail.

The Key Project has adopted an LMC distance modulus of 18.50 ± 0.10 mag. The review of published distances to the LMC, via various techniques, by Westerlund (1997) (his Table 2.8) indicates that the distance modulus to the LMC is still uncertain at the 0.10 mag level. More recently, Gould & Uza (1998), using observations of a light echo from Supernova 1987A, suggest an LMC distance modulus no larger than

18.37 ± 0.04 mag or 18.44 ± 0.05 mag for a circular or elliptical ring respectively. Panagia *et al.* (1998) used HST observations of the ring around SN 1987A to obtain an LMC distance modulus of 18.58 ± 0.05 mag. Work by Wood, Arnold, & Sebo (1997) using models of the LMC Cepheid HV 905 produced an LMC distance modulus of 18.51 ± 0.05 mag. Recent results from the MACHO Project (Alcock *et al.* 1997) using double mode RR Lyrae stars give an LMC distance modulus of 18.48 ± 0.19 mag. In light of these recent results we feel that our adopted LMC distance modulus and error are still valid.

Madore & Freedman (1991) fit Cepheid PL relations to 32 LMC Cepheids using *BVRI* photoelectric photometry. The dispersions for a single point about the PL relations are ± 0.27 mag for *V* and ± 0.18 mag for *I*. The PL zero point errors are obtained by dividing by the square root of the number of Cepheids used in the fit, giving us ± 0.05 mag for *V* and ± 0.03 for *I*, items (2) and (3) in Table 8.

The LMC distance modulus and PL relation zero point uncertainties are sources of systematic error within the Key Project, since we use the Madore & Freedman equations for all of the galaxies, and all galaxy determinations will change systematically as improvements to the zero point become available. Combining items (1), (2), and (3) in Table 8 in quadrature we obtain a PL relation uncertainty of ± 0.12 mag.

Hill *et al.* (1998) estimated our WFPC2 zero point uncertainties to be ± 0.02 mag for both *V* and *I* by comparing ground-based and HST observations of M100. In addition we must include the uncertainties in the aperture corrections. While there is one case where two aperture corrections within an epoch differed by 0.3 mag (Chip 1 *I* band, first epoch), the scatter about the mean ALLFRAME aperture corrections is ± 0.07 mag for *V* and ± 0.06 mag for *I*. We will take these to be the errors in zero point due to the aperture corrections. We then combine the Hill *et al.* errors and the aperture correction errors in quadrature to obtain WFPC2 zero point errors of ± 0.07 mag in *V* and ± 0.06 mag in *I*, items (4) and (5) in Table 8. Since the photometric errors in the two bands are uncorrelated we combine items (4) and (5) in quadrature, but we must weight these errors, σ_V and σ_I , by the differing effects of reddening, as given by $[(1 - R)^2(\sigma_V)^2 + R^2(\sigma_I)^2]^{1/2}$. As stated previously, we have adopted a reddening law of $R_V = A_V/E(V - I) = 2.45$. Our photometric contribution to the error in the distance modulus is therefore ± 0.18 mag.

Early work by the Key Project discovered what appeared to be a long versus short exposure zero point offset, such that stars in exposures longer than approximately 1000 seconds were systematically brighter, by approximately 0.05 mag, than stars in exposures of less than 1000 seconds duration. The effect is now thought to be a charge transfer efficiency effect in the WFPC2 CCDs. This effect is discussed in detail in Hill *et al.* (1998) and also in Whitmore & Heyer (1997). For the Key Project we have used the long exposure zero point for our photometric calibration. At this time, an offset of +0.05 mag for both *V* and *I* is thought to be the best estimate to correct for this effect. Additional work on the zero points is currently being undertaken by Stetson *et al.* (1998b) based on an extensive set of ground based and HST data. This effect is included in Table 8 as a source of systematic error in the distance to NGC 1365.

There is an additional distance modulus error introduced from fitting the Cepheid PL relations. From Section 5, these errors are ± 0.05 mag in *V* and ± 0.06 mag in *I*, and include photometric errors, differential reddening and the apparent width of the instability strip in both *V* and *I*. These errors are combined in quadrature in item (R2) in Table 8.

There is concern that the Cepheid PL relation may have a metallicity dependence. The Cepheids in the calibrating LMC are thought to be relatively metal poor compared Fornax and Virgo cluster galaxies (Kennicutt *et al.* 1998), so a metallicity dependence in the Cepheid PL relation would be a source of systematic error in our distance determination. Kennicutt *et al.* measured a marginal metallicity dependence in one of the Key Project galaxies, M101, leading to a shift in distance modulus of

$\delta(m - M)_0/\delta[O/H] = -0.24 \pm 0.16$ mag/dex. We can use this relation to estimate the systematic error in distance modulus to NGC 1365 due to a metallicity dependence on the Cepheid PL relations. Zaritsky, Kennicutt & Huchra (1994) found the oxygen abundance in NGC 1365 to be $12 + \log(O/H) = 9.0$ while the measured oxygen abundance in the LMC on this scale is $12 + \log(O/H) = 8.50$ (Kennicutt *et al.* 1998). The 0.5 dex difference in oxygen abundance would, if applied, increase the true distance modulus by +0.12 mag or a 6% increase in the distance to NGC 1365.

The total uncertainty in distance modulus to NGC 1365 due to random errors is obtained by combining the distance modulus and PL fit uncertainties in quadrature: $[0.18^2 + 0.08^2]^{1/2} = \pm 0.20$ mag.

The total systematic error in the distance to NGC 1365 is obtained by combining the systematic errors, the LMC Cepheid PL relation, a possible metallicity dependence, and the long versus short exposure zero point, in quadrature: $[0.12^2 + 0.12^2 + 0.05^2]^{1/2} = \pm 0.18$ mag. Thus our final distance modulus to NGC 1365 is 31.31 ± 0.20 (random) ± 0.18 (systematic). The implications of a Cepheid distance to NGC 1365 and the Fornax cluster are discussed in the companion paper Madore *et al.* (1998).

7. Conclusion

We have used the HST WFPC2 instrument to obtain 12 epochs in *V* and 4 epochs in *I* of the eastern part of NGC 1365 located in the Fornax Cluster. The images were reduced separately using the ALLFRAME and DoPHOT photometry packages. The raw photometry was transformed to standard Johnson *V* and Cousins *I* photometry via Hill *et al.* (1998) zero points, Holtzman *et al.* (1995a) color terms, and aperture corrections derived from the NGC 1365 images. The $\lesssim 0.1$ mag difference between the final ALLFRAME and DoPHOT photometry is most likely due to the relatively large uncertainties in both the ALLFRAME and DoPHOT aperture corrections, which show a scatter of ± 0.07 mag.

A total of 52 Cepheids were discovered in NGC 1365, ranging in period from 14 to 60 days. A subset of 34 Cepheids was chosen based on period, light curve shape, color and relative crowding to fit Cepheid period-luminosity relations using fixed slopes from Madore & Freedman (1991). A distance modulus of 31.31 ± 0.20 (random) ± 0.18 (systematic) mag, corresponding to 18.3 ± 1.7 (random) ± 1.6 (systematic) Mpc is obtained from the ALLFRAME photometry. A distance modulus of 31.26 ± 0.10 mag (internal errors only) was obtained from the DoPHOT photometry. The average reddening in this region of NGC 1365 was measured to be $E(V-I) = 0.16 \pm 0.08$ mag using ALLFRAME and 0.15 ± 0.10 mag using DoPHOT. The apparent agreement in distance between ALLFRAME and DoPHOT despite the observed $\lesssim 0.1$ mag photometric differences is due to DoPHOT measuring a lower reddening to NGC 1365 in WFPC2 Chips 1, 3 and 4 and a higher reddening than ALLFRAME in Chip 2. Over one-third of the Cepheids in the PL fit sample are found in Chip 2, reducing the *mean* difference in reddening and distance modulus between DoPHOT and ALLFRAME. The companion paper by Madore *et al.* (1998) discusses in detail the implications of a Cepheid distance to NGC 1365.

The work presented in this paper is based on observations made by the NASA/ESA Hubble Space Telescope, obtained by the Space Telescope Science Institute, which is operated by AURA, Inc. under NASA contract No. 5-26555. We gratefully acknowledge the support of the NASA and STScI support staff, with special thanks our program coordinator, Doug Van Orsow. Support for this work was provided by NASA through grant GO-2227-87A from STScI. This paper is based partially on data obtained at the Las Campanas Observatory 2.5m telescope in Chile, owned and operated by the Carnegie Institution

of Washington. SMGH and PBS are grateful to NATO for travel support via a Collaborative Research Grant (960178). LF acknowledges support by NASA through Hubble Fellowship grant HF-01081.01-96A awarded by the Space Telescope Science Institute, which is operated by AURA, Inc., for NASA under contract NSA 5-26555. The research described in this paper was partially carried out by the Jet Propulsion Laboratory, California Institute of Technology, under a contract with the National Aeronautics and Space Administration. This research has made use of the NASA/IPAC Extragalactic Database (NED) which is operated by the Jet Propulsion Laboratory, California Institute of Technology, under a contract with the National Aeronautics and Space Administration.

A. Appendix

A.1. Secondary Standard Photometry

Several bright stars in each WFPC2 field were used to determine the ALLFRAME aperture corrections. These relatively isolated stars are presented here as secondary standards for our NGC 1365 HST field.

A.2. Possible Variable Stars

There are several stars within the ALLFRAME and DoPHOT datasets that appear to be variable but for one reason or another did not make it into our list of definite Cepheids. Reasons may include uncertain periods, too crowded, extremely red or blue, or the variability is seen in either the ALLFRAME or DoPHOT dataset but not both. Positions, ALLFRAME mean V and I intensity averaged magnitudes, and possible periods for these stars are given in the table below.

REFERENCES

- Alcock, C., *et al.*, 1997, ApJ, 482, 89
- Bureau, M., Mould, J. R., & Staveley-Smith, L. 1996, ApJ, 463, 60
- Burrows, C. J., *et al.* 1994, Wide Field and Planetary Camera 2 Instrument Handbook (Baltimore: STScI)
- Cardelli, J. A., Clayton, G. C., & Mathis, J. S. 1989, ApJ, 345, 245
- Dean, J. F., Warren, P. R., & Cousins, A. W. 1978, MNRAS, 183, 569
- de Vaucouleurs, G., de Vaucouleurs, A., Corwin, H. G., Buta, R. J., Paturel, G., & Fouque, P. 1991, Third Reference Catalogue of Bright Galaxies (New York: Springer-Verlag)
- Ferrarese, L., *et al.* 1996, ApJ, 464, 568
- Ferrarese, L., *et al.* 1998a, ApJ, in press, astro-ph/9805365
- Ferrarese, L., *et al.* 1998b, in preparation
- Freedman, W. L., 1988, ApJ, 326, 691
- Freedman, W. L., *et al.* 1994, ApJ, 427, 628
- Graham, J.A., *et al.* 1997, ApJ, 477, 535
- Gould, A., & Uza, O. 1998, ApJ, 494, 118
- Held, E. V., & Mould, J.R. 1994, AJ, 107, 1307
- Hill, R., *et al.* 1998, ApJ, 496, 648
- Holtzman, J., *et al.* 1995a, PASP, 107, 1065
- Holtzman, J., *et al.* 1995b, PASP, 107, 156
- Hughes, S. M. G., *et al.* 1998, ApJ, in press
- Hughes, S. M. G., *et al.* 1994, ApJ, 428, 143
- Jörsäter, S. & van Moorsel, G. A. 1995, AJ, 110, 2037
- Kelson, D., *et al.* 1996, ApJ, 463, 26
- Kennicutt, R. C., Freedman, W. L., & Mould, J. R. 1995, AJ, 110, 1476
- Kennicutt, R. C., *et al.* 1998, ApJ, 498, 181
- Lafler, J., & Kinman, T. D. 1965, ApJS, 11, 216
- Madore, B. F., *et al.* 1998a, ApJ, in prep
- Madore, B. F., *et al.* 1998b, Nature, in press
- Madore, B. F., & Freedman, W. L. 1991, PASP, 103, 933
- McMillan, R., Ciardullo, R., & Jacoby, G. H. 1993, ApJ, 416, 62
- Mould, J. R. *et al.* 1998, in prep
- Panagia, N., *et al.* 1998, BAAS, 191, 1909
- Phelps, R., *et al.* 1998, ApJ, in press
- Prosser, C., *et al.* 1998, in prep
- Rawson, D., *et al.* 1997, ApJ, 490, 517
- Saha, A., & Hoessel, J. G. 1990, AJ, 99, 97

- Saha, A., *et al.* 1994, ApJ, 425, 14
- Saha, A., *et al.* 1996, ApJ, 466, 55
- Schoniger, F., & Sofue, Y. 1994, A&A, 283, 21
- Sandage, A., & Tammann, G. A. 1981, A Revised Shapley-Ames Catalog of Bright Galaxies, (Washington D.C.: Carnegie Institution of Washington)
- Schechter, P. L., Mateo, M., & Saha, A. 1993, PASP, 105, 1342
- Silbermann, N. A., *et al.* 1996, ApJ, 470, 1
- Stanek, K. Z. 1996, ApJ, 460, L37
- Stellingwerf, R. F. 1978, ApJ, 224, 953
- Stetson, P. B. 1987, PASP, 99, 191
- Stetson, P. B. 1990, PASP, 102, 932
- Stetson, P. B. 1991, in Third ESO/ST-ECF Data Analysis Workshop, ed. P. J. Grosbol & R. H. Warmels (Garching, ESO), 187
- Stetson, P. B. 1992, Astronomical Data Analysis Software and Systems I, ed. D. M. Worrall, C. Biemesderfer, & J. Barnes (San Francisco, ASP), ASP Conf. Ser., 25, 297
- Stetson, P. B. 1993, in Stellar Photometry - Current Techniques and Future Developments, IAU Coll. Ser., 136, (Cambridge, Cambridge University Press), 291
- Stetson, P. B. 1994, PASP, 106, 250
- Stetson, P. B., Davis, L. E., & Crabtree, D. R. 1990, in CCDs in Astronomy, ed. G. H. Jacoby, ASP Conf. Ser., 8, (San Francisco, ASP), 289
- Stetson, P. B., *et al.* 1998a, in preparation
- Stetson, P. B., *et al.* 1998b, in preparation
- Turner, A., *et al.* 1998, ApJ, in press
- Veron, P., Linblad, P. O., Zuiderwijk, E. J., Adam, G., & Veron, M. P. 1980, A&A, 87, 245
- Welch, D. L., & Stetson, P. B. 1993, AJ, 105, 1813
- Westerlund, B. E. 1997, The Magellanic Clouds, Cambridge Astrophysics Series No. 29, (Cambridge: Cambridge University Press), 20
- Whitmore, B. C., & Heyer, I. 1997, in HST Instrument Science Report WFPC2 97-08 (Space Telescope Science Institute, Baltimore)
- Wood, P. R., Arnold, A., & Sebo, K. M. 1997, ApJ, 485, 25
- Zaritsky, D., Kennicutt, R., & Huchra, J. 1994, ApJ, 420, 87

Table 1. HST Observations of NGC 1365

Image Identification	UT Day 1995	HJD 2449000.+	Exp. Time (seconds)	HST Filter
u2s70201t	Aug 6	936.1312	2400	F555W
u2s70202t	Aug 6	936.1961	2700	F555W
u2s70203t	Aug 6	936.2635	2700	F814W
u2s70204t	Aug 6	936.3301	2700	F814W
u2s70301t	Aug 14	943.9046	2400	F555W
u2s70302t	Aug 14	943.9688	2700	F555W
u2s70303t	Aug 15	944.0355	2700	F814W
u2s70304t	Aug 15	944.1028	2700	F814W
u2s70401t	Aug 21	951.2786	2400	F555W
u2s70402t	Aug 21	951.3407	2700	F555W
u2s70501t	Aug 24	953.6266	2400	F555W
u2s70502t	Aug 24	953.6915	2700	F555W
u2s70601t	Aug 26	956.1726	2400	F555W
u2s70602t	Aug 26	956.2362	2700	F555W
u2s70701t	Aug 29	959.1880	2400	F555W
u2s70703t	Aug 29	959.2583	2300	F555W
u2s70705t	Aug 29	959.3256	2300	F814W
u2s70706t	Aug 29	959.3897	2700	F814W
u2s70801t	Sept 1	962.2771	2400	F555W
u2s70802t	Sept 1	962.3413	2700	F555W
u2s70901t	Sept 5	966.6966	2400	F555W
u2s70902t	Sept 5	966.7602	2700	F555W
u2s71001t	Sept 8	969.3816	2400	F555W
u2s71002t	Sept 8	969.4465	2700	F555W
u2s71101t	Sept 13	974.2040	2400	F555W
u2s71102t	Sept 13	974.2717	2700	F555W
u2s71201t	Sept 19	980.2369	2400	F555W
u2s71202t	Sept 19	980.3026	2700	F555W
u2s71203t	Sept 19	980.3692	2700	F814W
u2s71204t	Sept 19	980.4359	2700	F814W
u2s71301t	Sept 24	985.2620	2400	F555W
u2s71302t	Sept 24	985.3277	2700	F555W

Table 2. DoPHOT vs ALLFRAME Photometry

Chip	Number of Stars	DoPHOT-ALLFRAME ΔV	Number of Stars	DoPHOT-ALLFRAME ΔI
bright non-variable stars				
1	103	$+0.13 \pm 0.04$	329	$+0.10 \pm 0.06$
2	332	$+0.02 \pm 0.06$	649	-0.11 ± 0.05
3	40	-0.09 ± 0.03	179	-0.15 ± 0.04
4	159	$+0.03 \pm 0.07$	401	-0.07 ± 0.04
Cepheids				
1	11	-0.01 ± 0.04	11	$+0.04 \pm 0.04$
2	12	-0.14 ± 0.02	12	-0.18 ± 0.02
3	8	-0.11 ± 0.02	8	-0.11 ± 0.05
4	6	-0.08 ± 0.05	6	-0.05 ± 0.06

Table 3. Positions and Periods of NGC 1365 Cepheids

ID	Chip	x	y	RA(J2000)	Dec(J2000)	P(days)	σ P	logP
V1	1	501.7	245.8	3:33:43.72	-36:09:21.6	60.0	...	1.78
V2	4	480.7	446.9	3:33:45.28	-36:10:13.6	60.0	...	1.78
V3	3	451.6	481.6	3:33:50.44	-36:09:20.7	55.0	...	1.74
V4	1	769.4	428.3	3:33:42.51	-36:09:23.2	55.0	...	1.74
V5	1	294.4	183.4	3:33:44.47	-36:09:17.7	53.0	...	1.72
V6	1	590.2	423.4	3:33:43.04	-36:09:18.1	47.0	4.0	1.67
V7	4	415.3	666.8	3:33:43.55	-36:10:22.7	44.2	5.2	1.65
V8	4	479.5	486.8	3:33:45.03	-36:10:16.1	42.5	4.5	1.63
V9	1	428.2	228.2	3:33:43.98	-36:09:20.1	41.5	3.5	1.62
V10	3	513.3	457.7	3:33:50.70	-36:09:14.9	41.4	3.6	1.62
V11	2	424.5	287.5	3:33:45.13	-36:08:29.7	41.0	7.0	1.61
V12	2	400.9	617.7	3:33:47.31	-36:08:10.0	39.2	4.8	1.59
V13	2	89.5	378.2	3:33:47.49	-36:08:49.1	38.0	4.0	1.58
V14	3	200.5	285.7	3:33:47.82	-36:09:22.1	37.6	2.6	1.58
V15	4	586.4	695.2	3:33:44.27	-36:10:37.6	35.2	1.2	1.55
V16	1	456.2	724.5	3:33:42.69	-36:09:03.7	35.1	3.1	1.55
V17	2	244.1	571.1	3:33:47.86	-36:08:24.9	35.0	1.5	1.54
V18	3	130.3	732.3	3:33:49.76	-36:10:00.4	34.6	1.9	1.54
V19	1	162.7	432.9	3:33:44.24	-36:09:05.1	34.5	4.5	1.54
V20	2	423.6	663.7	3:33:47.47	-36:08:05.3	34.4	4.4	1.54
V21	3	311.8	612.5	3:33:50.26	-36:09:39.6	34.0	2.0	1.53
V22	3	120.6	226.0	3:33:47.00	-36:09:22.7	34.0	2.5	1.53
V23	1	691.8	112.0	3:33:43.50	-36:09:31.9	34.0	2.3	1.53
V24	4	500.6	464.7	3:33:45.28	-36:10:16.3	33.6	0.6	1.53
V25	1	292.1	430.9	3:33:43.87	-36:09:09.0	33.1	2.5	1.52
V26	2	306.0	619.8	3:33:47.83	-36:08:17.0	32.5	2.5	1.51
V27	2	424.3	574.6	3:33:46.91	-36:08:11.1	31.3	3.3	1.50
V28	3	449.9	396.8	3:33:49.97	-36:09:14.4	30.3	4.0	1.48
V29	4	156.9	595.9	3:33:42.63	-36:09:58.4	29.8	4.2	1.47
V30	2	438.1	139.8	3:33:44.13	-36:08:38.3	29.6	2.7	1.47
V31	4	390.7	359.9	3:33:45.36	-36:10:01.2	29.0	2.3	1.46
V32	3	392.3	339.6	3:33:49.31	-36:09:13.8	28.9	2.2	1.46
V33	2	517.7	39.1	3:33:43.08	-36:08:38.9	28.0	2.0	1.45
V34	1	706.4	473.5	3:33:42.58	-36:09:19.7	28.0	3.0	1.45
V35	4	295.8	123.9	3:33:46.35	-36:09:38.8	27.5	4.0	1.44
V36	2	395.2	170.1	3:33:44.55	-36:08:39.6	26.6	2.6	1.42
V37	4	168.9	545.3	3:33:43.02	-36:09:56.1	26.5	1.5	1.42
V38	3	630.0	499.6	3:33:51.65	-36:09:10.5	26.5	1.5	1.42
V39	2	170.5	478.3	3:33:47.68	-36:08:36.4	26.1	3.9	1.42
V40	1	774.3	292.5	3:33:42.83	-36:09:28.0	25.0	1.0	1.40
V41	1	744.9	158.7	3:33:43.24	-36:09:31.8	23.5	1.0	1.37

Table 3—Continued

ID	Chip	x	y	RA(J2000)	Dec(J2000)	P(days)	σ P	logP
V42	2	82.7	366.7	3:33:47.45	-36:08:50.3	22.9	1.9	1.36
V43	2	417.5	622.9	3:33:47.25	-36:08:08.4	21.0	1.0	1.32
V44	2	604.4	610.8	3:33:46.17	-36:07:55.1	21.0	0.7	1.32
V45	2	542.6	690.6	3:33:47.00	-36:07:54.6	20.3	1.4	1.31
V46	1	247.1	124.1	3:33:44.75	-36:09:18.3	20.1	1.6	1.30
V47	3	238.4	609.4	3:33:49.79	-36:09:44.1	20.0	1.0	1.30
V48	4	159.0	93.6	3:33:45.82	-36:09:26.4	18.8	1.1	1.27
V49	1	475.3	217.9	3:33:43.86	-36:09:21.8	18.0	0.6	1.26
V50	4	233.5	632.1	3:33:42.81	-36:10:06.6	16.3	1.7	1.21
V51	3	256.1	465.1	3:33:49.13	-36:09:32.1	16.2	0.3	1.21
V52	3	322.7	187.8	3:33:48.07	-36:09:06.8	14.2	0.4	1.15

Table 4. V Photometry for NGC 1365 Cepheids

Cepheid	Heliocentric Julian Date 2449000.+					
	936.164	943.937	951.310	953.659	956.204	959.223
V1	25.29 ± 0.12	25.21 ± 0.13	25.47 ± 0.19	25.50 ± 0.14	25.44 ± 0.17	25.49 ± 0.16
V2	25.40 ± 0.19	25.22 ± 0.13	24.76 ± 0.15	24.63 ± 0.14	24.61 ± 0.14	24.62 ± 0.13
V3	25.44 ± 0.13	25.20 ± 0.15	24.38 ± 0.19	24.53 ± 0.14	24.50 ± 0.11	24.43 ± 0.12
V4	25.31 ± 0.15	25.37 ± 0.16	25.66 ± 0.17	25.62 ± 0.26	25.63 ± 0.20	25.69 ± 0.16
V5	25.86 ± 0.15	25.97 ± 0.17	26.29 ± 0.21	26.29 ± 0.16	26.12 ± 0.20	26.33 ± 0.24
V6	26.44 ± 0.26	25.90 ± 0.26	25.68 ± 0.16	25.57 ± 0.14	25.57 ± 0.21	25.94 ± 0.20
V7	26.23 ± 0.29	25.02 ± 0.12	25.32 ± 0.17	25.47 ± 0.13	25.57 ± 0.16	25.54 ± 0.13
V8	26.02 ± 0.15	25.04 ± 0.13	25.35 ± 0.18	25.44 ± 0.16	25.58 ± 0.16	25.50 ± 0.15
V9	25.95 ± 0.18	26.27 ± 0.19	26.21 ± 0.19	...	25.21 ± 0.45	25.50 ± 0.14
V10	25.72 ± 0.15	25.56 ± 0.29	26.00 ± 0.20	...	25.97 ± 0.15	26.03 ± 0.19
V11	26.65 ± 0.35	27.01 ± 0.48	27.16 ± 0.63	26.12 ± 0.26	26.02 ± 0.25	25.97 ± 0.21
V12	26.18 ± 0.21	25.52 ± 0.15	25.80 ± 0.19	25.97 ± 0.18	25.99 ± 0.17	25.79 ± 0.13
V13	25.84 ± 0.18	26.17 ± 0.20	26.62 ± 0.31	26.52 ± 0.29	26.74 ± 0.32	26.73 ± 0.29
V14	26.73 ± 0.22	26.85 ± 0.30	26.02 ± 0.17	26.25 ± 0.20	26.17 ± 0.17	26.06 ± 0.52
V15	26.12 ± 0.17	26.34 ± 0.21	25.62 ± 0.19	25.66 ± 0.20	25.59 ± 0.16	25.68 ± 0.16
V16	25.78 ± 0.19	25.86 ± 0.16	26.07 ± 0.24	26.32 ± 0.22	26.32 ± 0.23	26.15 ± 0.20
V17	25.97 ± 0.15	26.15 ± 0.24	25.12 ± 0.16	25.21 ± 0.27	25.38 ± 0.18	25.35 ± 0.14
V18	25.53 ± 0.13	25.80 ± 0.18	26.24 ± 0.40	26.34 ± 0.25	26.16 ± 0.17	25.70 ± 0.14
V19	25.97 ± 0.19	26.47 ± 0.21	26.72 ± 0.30	26.57 ± 0.25	26.42 ± 0.23	25.66 ± 0.18
V20	26.38 ± 0.16	26.84 ± 0.26	25.77 ± 0.15	25.48 ± 0.13	25.65 ± 0.16	25.84 ± 0.16
V21	25.76 ± 0.16	25.89 ± 0.23	26.30 ± 0.22	26.53 ± 0.21	26.52 ± 0.20	26.24 ± 0.16
V22	26.29 ± 0.41	25.66 ± 0.15	25.77 ± 0.15	25.81 ± 0.19	25.79 ± 0.17	25.88 ± 0.15
V23	26.19 ± 0.17	25.29 ± 0.13	25.68 ± 0.17	26.02 ± 0.23	25.76 ± 0.15	25.89 ± 0.19
V24	26.22 ± 0.19	26.74 ± 0.30	...	25.82 ± 0.16	25.64 ± 0.46	25.59 ± 0.22
V25	26.06 ± 0.18	26.58 ± 0.22	25.31 ± 0.13	25.55 ± 0.16	25.52 ± 0.16	25.81 ± 0.15
V26	25.53 ± 0.17	25.82 ± 0.19	26.23 ± 0.24	26.40 ± 0.25	26.33 ± 0.31	25.51 ± 0.16
V27	26.61 ± 0.24	25.49 ± 0.13	26.10 ± 0.23	26.26 ± 0.19	26.34 ± 0.19	26.33 ± 0.26
V28	26.67 ± 0.23	26.64 ± 0.23	26.43 ± 0.26	26.21 ± 0.18	26.41 ± 0.15	26.36 ± 0.19
V29	26.32 ± 0.26	26.45 ± 0.21	25.60 ± 0.19	25.67 ± 0.18	25.72 ± 0.16	25.78 ± 0.18
V30	25.56 ± 0.16	25.84 ± 0.21	25.98 ± 0.23	25.55 ± 0.23	25.05 ± 0.13	24.87 ± 0.35
V31	25.73 ± 0.32	26.56 ± 0.19	26.70 ± 0.27	26.09 ± 0.24	25.61 ± 0.15	25.72 ± 0.15
V32	...	26.58 ± 0.23	26.35 ± 0.22	26.81 ± 0.28	26.75 ± 0.24	26.77 ± 0.28
V33	25.77 ± 0.22	25.79 ± 0.29	25.65 ± 0.63	25.79 ± 0.33	25.27 ± 0.23	25.40 ± 0.19
V34	25.81 ± 0.55	26.10 ± 0.25	25.63 ± 0.16	25.65 ± 0.13	25.71 ± 0.16	25.74 ± 0.32
V35	26.80 ± 0.26	27.11 ± 0.25	25.99 ± 0.27	26.21 ± 0.19	26.16 ± 0.18	26.44 ± 0.23
V36	26.77 ± 0.41	26.00 ± 0.22	26.73 ± 0.37	26.58 ± 0.52	26.47 ± 0.25	26.94 ± 0.33
V37	25.69 ± 0.15	26.24 ± 0.22	27.12 ± 0.45	26.88 ± 0.31	26.47 ± 0.27	25.72 ± 0.31
V38	26.79 ± 0.25	25.95 ± 0.18	26.49 ± 0.19	26.50 ± 0.18	26.49 ± 0.35	26.53 ± 0.22
V39	26.44 ± 0.24	25.62 ± 0.15	26.17 ± 0.22	26.39 ± 0.19	26.58 ± 0.23	26.39 ± 0.21
V40	25.46 ± 0.31	25.88 ± 0.26	26.24 ± 0.35	26.26 ± 0.35	26.32 ± 0.44	26.30 ± 0.33

Table 4—Continued

Cepheid	Heliocentric Julian Date 2449000.+					
	936.164	943.937	951.310	953.659	956.204	959.223
V41	26.05 ± 0.22	25.36 ± 0.15	26.07 ± 0.30	26.15 ± 0.28	26.16 ± 0.23	26.14 ± 0.25
V42	26.37 ± 0.19	25.59 ± 0.14	26.28 ± 0.19	26.25 ± 0.21	26.34 ± 0.27	26.47 ± 0.25
V43	26.48 ± 0.24	26.13 ± 0.20	26.58 ± 0.27	26.62 ± 0.25	26.10 ± 0.46	25.62 ± 0.47
V44	26.95 ± 0.26	26.22 ± 0.20	27.53 ± 0.52	27.18 ± 0.38	27.08 ± 0.37	25.73 ± 0.14
V45	27.36 ± 0.57	26.48 ± 0.19	27.06 ± 0.37	27.16 ± 0.36	27.33 ± 0.45	27.11 ± 0.38
V46	26.75 ± 0.23	25.65 ± 0.14	26.32 ± 0.18	26.63 ± 0.21	26.53 ± 0.50	26.61 ± 0.70
V47	25.93 ± 0.15	26.42 ± 0.18	26.45 ± 0.36	25.77 ± 0.17	26.04 ± 0.18	25.81 ± 0.44
V48	26.08 ± 0.17	26.89 ± 0.26	27.11 ± 0.31	25.94 ± 0.18	26.24 ± 0.14	26.46 ± 0.25
V49	26.63 ± 0.25	27.17 ± 0.40	26.44 ± 0.23	26.50 ± 0.25	26.96 ± 0.29	27.20 ± 0.33
V50	26.66 ± 0.28	26.37 ± 0.24	26.69 ± 0.29	26.80 ± 0.26	27.07 ± 0.37	26.93 ± 0.35
V51	26.97 ± 0.28	26.86 ± 0.47	27.45 ± 0.47	26.49 ± 0.21	26.79 ± 0.36	26.74 ± 0.21
V52	27.36 ± 0.34	26.55 ± 0.21	27.12 ± 0.32	27.59 ± 0.47	26.31 ± 0.21	26.42 ± 0.21

Table 4. V Photometry for NGC 1365 Cepheids

Cepheid	Heliocentric Julian Date 2449000.+					
	962.309	965.728	969.414	974.238	980.270	985.295
V1	25.48 ± 0.13	25.66 ± 0.13	25.65 ± 0.13	25.90 ± 0.14	25.94 ± 0.18	26.06 ± 0.19
V2	24.61 ± 0.12	24.75 ± 0.11	24.76 ± 0.12	24.80 ± 0.13	24.99 ± 0.11	25.00 ± 0.14
V3	24.65 ± 0.12	24.80 ± 0.11	24.75 ± 0.22	24.81 ± 0.11	24.96 ± 0.12	25.16 ± 0.13
V4	25.80 ± 0.16	25.71 ± 0.15	25.73 ± 0.17	25.44 ± 0.13	25.17 ± 0.14	25.20 ± 0.14
V5	26.35 ± 0.45	26.47 ± 0.31	26.68 ± 0.17	26.48 ± 0.21	25.53 ± 0.31	25.79 ± 0.17
V6	25.86 ± 0.21	25.98 ± 0.18	26.11 ± 0.19	26.19 ± 0.18	26.61 ± 0.26	26.16 ± 0.20
V7	25.61 ± 0.35	25.53 ± 0.42	25.85 ± 0.32	26.14 ± 0.17	26.06 ± 0.16	24.70 ± 0.17
V8	25.62 ± 0.31	25.97 ± 0.18	25.88 ± 0.18	25.99 ± 0.20	26.09 ± 0.20	24.94 ± 0.14
V9	25.43 ± 0.16	25.62 ± 0.15	25.77 ± 0.14	25.78 ± 0.17	26.07 ± 0.17	26.24 ± 0.21
V10	26.01 ± 0.14	26.26 ± 0.20	26.29 ± 0.17	26.23 ± 0.15	25.68 ± 0.17	25.61 ± 0.14
V11	26.16 ± 0.23	26.19 ± 0.22	26.16 ± 0.24	26.60 ± 0.30	26.48 ± 0.74	27.09 ± 0.39
V12	25.99 ± 0.18	25.99 ± 0.19	26.27 ± 0.24	26.21 ± 0.17	26.07 ± 0.20	25.38 ± 0.12
V13	26.64 ± 0.49	26.07 ± 0.17	25.80 ± 0.15	25.87 ± 0.16	26.11 ± 0.23	26.27 ± 0.23
V14	26.58 ± 0.17	26.65 ± 0.24	26.68 ± 0.62	26.74 ± 0.29	...	25.95 ± 0.14
V15	...	26.08 ± 0.21	25.94 ± 0.19	26.26 ± 0.19	26.09 ± 0.21	25.70 ± 0.16
V16	26.48 ± 0.37	26.50 ± 0.23	25.64 ± 0.16	25.46 ± 0.36	26.05 ± 0.20	26.10 ± 0.22
V17	25.50 ± 0.21	25.63 ± 0.14	25.77 ± 0.14	25.88 ± 0.15	26.02 ± 0.19	25.50 ± 0.16
V18	25.52 ± 0.13	25.43 ± 0.26	25.46 ± 0.14	25.59 ± 0.13	25.81 ± 0.13	26.14 ± 0.19
V19	25.77 ± 0.15	25.55 ± 0.36	25.78 ± 0.43	26.10 ± 0.37	26.45 ± 0.22	26.65 ± 0.24
V20	25.83 ± 0.22	25.99 ± 0.30	26.21 ± 0.23	26.12 ± 0.53	26.64 ± 0.38	25.43 ± 0.29
V21	26.61 ± 0.22	26.53 ± 0.22	25.86 ± 0.15	25.71 ± 0.12	26.23 ± 0.17	26.27 ± 0.16
V22	26.05 ± 0.15	26.29 ± 0.18	26.35 ± 0.17	26.44 ± 0.27	25.38 ± 0.13	25.61 ± 0.37
V23	25.91 ± 0.19	26.25 ± 0.35	26.12 ± 0.22	25.19 ± 0.14	25.42 ± 0.14	25.70 ± 0.13
V24	25.91 ± 0.15	26.09 ± 0.18	26.16 ± 0.17	26.51 ± 0.32	26.77 ± 0.70	26.02 ± 0.21
V25	26.06 ± 0.18	26.16 ± 0.22	26.24 ± 0.23	26.39 ± 0.23	25.91 ± 0.18	25.49 ± 0.17
V26	25.29 ± 0.16	25.48 ± 0.18	25.56 ± 0.31	25.75 ± 0.17	25.86 ± 0.21	26.33 ± 0.24
V27	26.35 ± 0.21	26.82 ± 0.22	25.48 ± 0.12	25.42 ± 0.13	25.76 ± 0.41	25.98 ± 0.21
V28	26.52 ± 0.18	26.71 ± 0.21	26.54 ± 0.15	26.19 ± 0.20	26.08 ± 0.21	26.27 ± 0.21
V29	26.19 ± 0.16	26.44 ± 0.27	26.27 ± 0.28	26.39 ± 0.20	25.40 ± 0.12	25.63 ± 0.19
V30	25.16 ± 0.22	25.74 ± 0.19	25.82 ± 0.18	25.89 ± 0.19	26.00 ± 0.24	25.05 ± 0.26
V31	25.83 ± 0.13	26.32 ± 0.20	26.15 ± 0.15	26.16 ± 0.16	26.62 ± 0.26	25.46 ± 0.14
V32	27.03 ± 0.37	27.46 ± 0.48	26.99 ± 0.26	25.95 ± 0.16	26.49 ± 0.22	26.61 ± 0.30
V33	25.66 ± 0.28	25.66 ± 0.24	25.77 ± 0.26	26.14 ± 0.34	25.89 ± 0.34	25.25 ± 0.17
V34	25.85 ± 0.21	26.11 ± 0.23	26.35 ± 0.23	26.25 ± 0.21	25.59 ± 0.17	25.56 ± 0.29
V35	26.84 ± 0.41	26.79 ± 0.30	26.55 ± 0.25	26.90 ± 0.23	25.95 ± 0.18	26.30 ± 0.17
V36	26.70 ± 0.28	25.83 ± 0.15	25.86 ± 0.18	26.27 ± 0.33	26.89 ± 0.39	26.89 ± 0.31
V37	25.92 ± 0.16	26.12 ± 0.23	26.48 ± 0.21	26.55 ± 0.49	...	26.30 ± 0.21
V38	26.49 ± 0.17	25.67 ± 0.14	25.83 ± 0.15	25.92 ± 0.34	26.49 ± 0.19	26.66 ± 0.23
V39	26.53 ± 0.21	25.85 ± 0.15	25.66 ± 0.14	26.14 ± 0.20	26.48 ± 0.23	26.60 ± 0.20
V40	25.68 ± 0.17	25.92 ± 0.24	25.94 ± 0.19	26.22 ± 0.25	26.30 ± 0.29	25.54 ± 0.22

Table 4—Continued

Cepheid	Heliocentric Julian Date 2449000.+					
	962.309	965.728	969.414	974.238	980.270	985.295
V41	25.51 ± 0.23	25.61 ± 0.38	25.96 ± 0.21	26.03 ± 0.25	25.89 ± 0.17	25.57 ± 0.22
V42	26.58 ± 0.24	25.46 ± 0.14	25.88 ± 0.16	26.08 ± 0.14	26.47 ± 0.20	26.55 ± 0.22
V43	25.63 ± 0.13	26.12 ± 0.41	26.20 ± 0.19	26.54 ± 0.21	25.97 ± 0.17	25.39 ± 0.34
V44	26.05 ± 0.18	26.46 ± 0.22	26.89 ± 0.47	26.88 ± 0.52	25.86 ± 0.14	26.18 ± 0.15
V45	26.39 ± 0.22	26.56 ± 0.20	26.73 ± 0.24	27.51 ± 0.50	26.78 ± 0.25	26.60 ± 0.20
V46	25.72 ± 0.16	25.97 ± 0.15	26.19 ± 0.43	26.72 ± 0.27	26.64 ± 0.22	25.81 ± 0.28
V47	25.88 ± 0.33	26.54 ± 0.25	26.51 ± 0.20	25.76 ± 0.16	26.12 ± 0.19	26.35 ± 0.19
V48	26.70 ± 0.23	27.08 ± 0.38	26.84 ± 0.28	26.17 ± 0.15	26.96 ± 0.32	26.98 ± 0.29
V49	26.94 ± 0.31	26.21 ± 0.16	26.58 ± 0.24	27.40 ± 0.33	27.28 ± 0.37	26.31 ± 0.20
V50	26.07 ± 0.17	26.58 ± 0.31	26.84 ± 0.27	26.81 ± 0.51	26.21 ± 0.24	26.85 ± 0.35
V51	26.93 ± 0.29	27.03 ± 0.29	26.53 ± 0.17	26.90 ± 0.21	27.10 ± 0.40	26.68 ± 0.24
V52	27.20 ± 0.31	27.39 ± 0.33	26.96 ± 0.29	26.51 ± 0.58	26.84 ± 0.23	26.61 ± 0.18

Table 5. I Photometry for NGC 1365 Cepheids

Cepheid	Heliocentric Julian Date 2449000.+			
	936.297	944.069	959.358	980.403
V1	24.26 ± 0.13	24.22 ± 0.12	24.37 ± 0.15	24.55 ± 0.17
V2	24.38 ± 0.13	24.35 ± 0.13	23.87 ± 0.12	24.05 ± 0.13
V3	24.30 ± 0.12	24.23 ± 0.17	23.87 ± 0.11	23.79 ± 0.26
V4	24.18 ± 0.19	24.24 ± 0.16	24.43 ± 0.15	24.12 ± 0.14
V5	24.54 ± 0.31	24.82 ± 0.16	25.26 ± 0.16	24.82 ± 0.15
V6	25.34 ± 0.24	25.25 ± 0.25	24.95 ± 0.18	25.29 ± 0.36
V7	25.07 ± 0.17	24.39 ± 0.13	24.51 ± 0.15	24.99 ± 0.18
V8	24.95 ± 0.15	24.31 ± 0.14	24.37 ± 0.20	24.90 ± 0.22
V9	24.84 ± 0.19	24.97 ± 0.18	24.65 ± 0.14	24.95 ± 0.25
V10	24.87 ± 0.15	24.68 ± 0.19	25.06 ± 0.15	24.86 ± 0.14
V11	25.14 ± 0.30	25.33 ± 0.23	24.87 ± 0.18	25.34 ± 0.25
V12	24.93 ± 0.18	24.58 ± 0.14	24.95 ± 0.19	24.99 ± 0.18
V13	25.06 ± 0.20	25.36 ± 0.18	25.82 ± 0.30	25.28 ± 0.25
V14	25.50 ± 0.22	25.59 ± 0.18	25.39 ± 0.20	25.04 ± 0.18
V15	25.01 ± 0.22	25.37 ± 0.21	24.64 ± 0.14	24.99 ± 0.24
V16	24.63 ± 0.21	24.46 ± 0.33	25.13 ± 0.20	24.73 ± 0.15
V17	24.92 ± 0.23	25.15 ± 0.17	24.34 ± 0.20	24.83 ± 0.14
V18	24.83 ± 0.16	25.01 ± 0.16	25.15 ± 0.17	24.97 ± 0.15
V19	25.01 ± 0.16	25.28 ± 0.19	24.94 ± 0.17	25.28 ± 0.21
V20	25.42 ± 0.19	25.32 ± 0.21	25.03 ± 0.15	25.08 ± 0.54
V21	24.95 ± 0.15	25.15 ± 0.17	24.68 ± 0.88	24.63 ± 0.36
V22	25.42 ± 0.22	24.92 ± 0.15	24.87 ± 0.14	24.75 ± 0.14
V23	25.16 ± 0.21	24.56 ± 0.18	25.01 ± 0.20	24.68 ± 0.16
V24	25.29 ± 0.19	25.52 ± 0.24	24.98 ± 0.15	25.68 ± 0.22
V25	25.04 ± 0.20	25.21 ± 0.29	24.88 ± 0.16	25.17 ± 0.18
V26	24.61 ± 0.21	24.66 ± 0.18	24.81 ± 0.19	24.54 ± 0.37
V27	25.49 ± 0.32	24.88 ± 0.17	25.07 ± 0.18	24.84 ± 0.17
V28	25.71 ± 0.25	25.97 ± 0.28	25.57 ± 0.16	25.31 ± 0.24
V29	25.11 ± 0.21	25.53 ± 0.30	24.72 ± 0.28	24.76 ± 0.17
V30	24.69 ± 0.16	24.97 ± 0.25	24.60 ± 0.18	25.19 ± 0.28
V31	24.90 ± 0.15	25.10 ± 0.26	24.87 ± 0.15	25.64 ± 0.25
V32	26.56 ± 0.48	26.21 ± 0.44	25.75 ± 0.20	25.53 ± 0.20
V33	24.53 ± 0.43	24.76 ± 0.28	24.58 ± 0.22	24.98 ± 0.45
V34	25.23 ± 0.24	25.30 ± 0.25	24.86 ± 0.23	25.00 ± 0.31
V35	25.66 ± 0.24	26.01 ± 0.28	25.35 ± 0.22	25.21 ± 0.22
V36	25.77 ± 0.34	25.35 ± 0.39	25.85 ± 0.34	25.62 ± 0.29
V37	25.13 ± 0.18	25.42 ± 0.23	25.18 ± 0.17	...
V38	25.79 ± 0.30	25.13 ± 0.17	25.71 ± 0.18	25.38 ± 0.19
V39	25.69 ± 0.29	24.87 ± 0.15	25.73 ± 0.29	25.30 ± 0.19
V40	24.72 ± 0.24	24.90 ± 0.26	25.26 ± 0.28	25.24 ± 0.29

Table 5—Continued

Cepheid	Heliocentric Julian Date 2449000.+			
	936.297	944.069	959.358	980.403
V41	25.27 ± 0.21	24.90 ± 0.17	25.24 ± 0.20	25.56 ± 0.32
V42	25.72 ± 0.25	25.11 ± 0.43	25.67 ± 0.24	25.64 ± 0.27
V43	25.33 ± 0.19	25.09 ± 0.41	25.14 ± 0.16	25.47 ± 0.18
V44	25.73 ± 0.28	25.44 ± 0.22	25.25 ± 0.17	25.51 ± 0.23
V45	26.04 ± 0.38	25.89 ± 0.28	26.18 ± 0.30	25.92 ± 0.31
V46	25.40 ± 0.19	24.98 ± 0.17	25.81 ± 0.29	25.65 ± 0.18
V47	24.87 ± 0.17	25.07 ± 0.26	25.01 ± 0.15	24.96 ± 0.18
V48	25.58 ± 0.18	25.72 ± 0.70	25.44 ± 0.49	25.82 ± 0.25
V49	25.55 ± 0.25	26.29 ± 0.37	25.95 ± 0.29	25.89 ± 0.23
V50	26.19 ± 0.60	26.01 ± 0.44	26.08 ± 0.52	25.74 ± 0.37
V51	26.36 ± 0.42	25.90 ± 0.29	26.00 ± 0.26	26.07 ± 0.27
V52	...	25.91 ± 0.25	25.87 ± 0.29	26.37 ± 0.39

Table 6. ALLFRAME Photometric Parameters for NGC 1365 Cepheids

ID	V_{int}	σ	V_{ph}	σ	I_{int}	σ	I_{ph}	σ	$(V - I)_{int}$	$(V - I)_{ph}$	PL
V1	25.62	0.07	25.66	0.07	24.41	0.07	24.40	0.07	1.21	1.25	
V2	24.88	0.07	25.00	0.08	24.07	0.12	24.16	0.11	0.80	0.84	
V3	24.85	0.09	24.96	0.10	23.96	0.12	24.03	0.11	0.89	0.93	
V4	25.55	0.06	25.52	0.06	24.32	0.07	24.29	0.06	1.22	1.23	
V5	26.22	0.09	26.21	0.09	25.03	0.15	24.98	0.14	1.20	1.23	
V6	26.05	0.09	26.08	0.09	25.10	0.09	25.19	0.08	0.95	0.90	+
V7	25.67	0.13	25.67	0.13	24.71	0.15	24.70	0.15	0.96	0.97	+
V8	25.68	0.11	25.70	0.11	24.64	0.15	24.60	0.15	1.04	1.10	
V9	25.87	0.10	25.91	0.11	24.80	0.07	24.83	0.06	1.07	1.08	+
V10	25.97	0.08	26.01	0.08	24.98	0.09	24.93	0.08	0.99	1.08	+
V11	26.55	0.12	26.60	0.12	25.17	0.10	25.14	0.10	1.38	1.46	+
V12	25.96	0.08	25.99	0.08	24.89	0.09	24.90	0.09	1.06	1.09	+
V13	26.33	0.10	26.34	0.10	25.45	0.14	25.52	0.15	0.88	0.82	+
V14	26.47	0.10	26.53	0.10	25.43	0.11	25.46	0.11	1.04	1.07	+
V15	25.95	0.08	25.99	0.08	24.96	0.13	24.96	0.13	0.99	1.03	+
V16	26.10	0.09	26.13	0.09	24.84	0.13	24.87	0.14	1.27	1.26	+
V17	25.67	0.09	25.71	0.10	24.72	0.15	24.78	0.15	0.95	0.94	+
V18	25.86	0.09	25.84	0.09	25.07	0.07	25.03	0.06	0.79	0.81	+
V19	26.25	0.12	26.23	0.12	25.17	0.08	25.11	0.08	1.08	1.11	+
V20	26.10	0.12	26.15	0.13	25.03	0.12	25.22	0.08	1.07	0.92	+
V21	26.25	0.09	26.27	0.09	24.97	0.12	24.85	0.10	1.27	1.42	+
V22	25.99	0.09	26.03	0.10	25.09	0.14	25.06	0.13	0.90	0.97	+
V23	25.83	0.10	25.84	0.10	24.92	0.12	24.95	0.13	0.92	0.88	+
V24	26.20	0.12	26.26	0.12	25.28	0.14	25.36	0.13	0.92	0.90	
V25	25.99	0.11	26.06	0.12	25.01	0.07	25.07	0.06	0.98	0.98	+
V26	25.90	0.11	25.87	0.11	24.77	0.08	24.69	0.05	1.14	1.17	+
V27	26.16	0.13	26.15	0.13	25.12	0.13	25.14	0.13	1.05	1.01	+
V28	26.44	0.06	26.46	0.06	25.65	0.12	25.68	0.12	0.78	0.78	
V29	26.05	0.11	26.09	0.11	25.07	0.16	25.09	0.17	0.98	1.00	
V30	25.61	0.11	25.65	0.12	24.87	0.12	24.91	0.12	0.74	0.74	
V31	26.15	0.12	26.18	0.12	25.13	0.15	25.21	0.16	1.02	0.97	+
V32	26.77	0.11	26.83	0.12	25.94	0.20	26.10	0.20	0.83	0.73	
V33	25.70	0.07	25.75	0.07	24.71	0.09	24.77	0.09	0.99	0.98	
V34	25.89	0.08	25.97	0.08	25.15	0.09	25.14	0.09	0.75	0.83	+
V35	26.57	0.11	26.63	0.11	25.55	0.15	25.65	0.16	1.01	0.98	+
V36	26.54	0.11	26.48	0.11	25.58	0.10	25.64	0.09	0.96	0.84	
V37	26.40	0.13	26.48	0.14	25.50	0.16	25.30	0.08	0.90	1.18	
V38	26.37	0.10	26.31	0.10	25.48	0.13	25.49	0.13	0.89	0.82	+
V39	26.29	0.10	26.25	0.10	25.45	0.18	25.37	0.17	0.84	0.87	+
V40	26.05	0.09	26.09	0.09	25.05	0.12	25.05	0.11	0.99	1.04	
V41	25.91	0.08	25.93	0.08	25.27	0.12	25.26	0.12	0.63	0.66	

Table 6—Continued

ID	V_{int}	σ	V_{ph}	σ	I_{int}	σ	I_{ph}	σ	$(V - I)_{int}$	$(V - I)_{ph}$	PL
V42	26.25	0.10	26.22	0.10	25.54	0.12	25.46	0.13	0.70	0.76	+
V43	26.18	0.11	26.21	0.12	25.31	0.08	25.26	0.07	0.87	0.95	+
V44	26.71	0.16	26.80	0.17	25.72	0.15	25.58	0.10	0.99	1.22	+
V45	26.99	0.11	26.97	0.11	26.01	0.06	26.00	0.06	0.97	0.97	+
V46	26.36	0.12	26.36	0.12	25.44	0.16	25.36	0.16	0.92	1.00	+
V47	26.17	0.09	26.23	0.09	25.02	0.04	25.00	0.04	1.15	1.23	+
V48	26.69	0.12	26.74	0.12	25.67	0.07	25.65	0.07	1.03	1.09	+
V49	26.87	0.11	26.85	0.11	25.84	0.14	25.84	0.14	1.03	1.01	+
V50	26.69	0.08	26.68	0.08	26.07	0.09	26.05	0.09	0.62	0.63	
V51	26.90	0.07	26.96	0.08	26.09	0.09	26.17	0.10	0.81	0.79	+
V52	26.99	0.12	27.06	0.13	26.27	0.18	26.16	0.15	0.73	0.90	

Table 7. Cepheid Distance Moduli to NGC 1365

Dataset	Chip	No.	μ_V	μ_I	A_V	μ_0
ALLFRAME Photometry						
phase	1	9	31.68	31.53	0.367	31.31
phase	2	12	31.72	31.55	0.408	31.31
phase	3	8	31.72	31.54	0.426	31.29
phase	4	5	31.71	31.55	0.382	31.33
phase	1-4	34	31.70	31.54	0.398	31.31
phase	1-4	52	31.68	31.54	0.331	31.35
phase	1,3,4	22	31.70	31.54	0.392	31.31
intensity	1	9	31.66	31.52	0.332	31.32
intensity	2	12	31.70	31.56	0.349	31.36
intensity	3	8	31.69	31.56	0.322	31.37
intensity	4	5	31.67	31.52	0.367	31.31
intensity	1-4	34	31.68	31.55	0.341	31.34
intensity	1-4	52	31.65	31.54	0.266	31.38
intensity	1,3,4	22	31.67	31.54	0.336	31.34
DoPHOT Photometry						
phase	1	9	31.63	31.52	0.280	31.35
phase	2	12	31.56	31.36	0.500	31.06
phase	3	8	31.79	31.63	0.397	31.39
phase	4	5	31.59	31.50	0.237	31.36
phase	1-4	34	31.64	31.49	0.379	31.26
phase	1-4	52	31.58	31.46	0.299	31.28
phase	1,3,4	22	31.68	31.55	0.313	31.37
intensity	1	9	31.63	31.51	0.285	31.34
intensity	2	12	31.57	31.37	0.478	31.09
intensity	3	8	31.77	31.62	0.366	31.41
intensity	4	5	31.59	31.48	0.260	31.33
intensity	1-4	34	31.64	31.48	0.369	31.27
intensity	1-4	52	31.58	31.46	0.297	31.28
intensity	1,3,4	22	31.67	31.55	0.309	31.36

Table 8. NGC 1365 Distance Modulus Error Budget

Source of Uncertainty	Error
Cepheid Period Luminosity Relation Calibration	
(1) LMC True Distance Modulus	± 0.10
(2) <i>V</i> -band PL Zero Point	± 0.05
(3) <i>I</i> -band PL Zero Point	± 0.03
(S1) PL Systematic Uncertainty	± 0.12
NGC 1365 Distance Modulus	
(4) HST WFPC2 <i>V</i> -band Photometry	± 0.07
(5) HST WFPC2 <i>I</i> -band Photometry	± 0.06
(R1) Cepheid True Modulus	± 0.18
NGC 1365 Cepheid PL Relation Fitting	
(6) <i>V</i> -band PL Fitting	± 0.05
(7) <i>I</i> -band PL Fitting	± 0.06
(R2) Cepheid True Modulus	± 0.08
(S2) Metallicity Uncertainty	± 0.12
(S3) Long vs Short Zero Point	± 0.05
Total Uncertainty	
(R) Random Errors	± 0.20
(S) Systematic Error	± 0.18

Table A1. Secondary Standard Stars in NGC 1365

Chip-ID	X	Y	RA (J2000)	Dec (J2000)	<i>V</i>	σ	<i>I</i>	σ
1-97	495.9	782.1	3:33:42.43	-36:09:02.8	24.28	0.10	23.13	0.10
1-101	515.3	592.1	3:33:42.84	-36:09:09.9	24.05	0.10	23.34	0.10
1-47	235.8	583.8	3:33:43.66	-36:09:02.0	23.38	0.10	23.13	0.10
1-78	313.2	555.3	3:33:43.50	-36:09:05.3	23.92	0.10	23.12	0.10
1-48	675.4	549.1	3:33:42.48	-36:09:16.2	23.59	0.10	22.70	0.10
1-83	778.9	412.7	3:33:42.52	-36:09:23.9	23.94	0.10	23.61	0.10
1-148	726.8	372.2	3:33:42.76	-36:09:23.8	24.37	0.10	23.52	0.10
1-5	123.0	290.2	3:33:44.69	-36:09:08.9	22.27	0.10	21.14	0.10
1-92	563.1	288.7	3:33:43.44	-36:09:21.9	23.89	0.10	23.93	0.11
1-105	702.2	251.3	3:33:43.13	-36:09:27.3	24.12	0.10	23.82	0.11
1-120	620.3	224.8	3:33:43.43	-36:09:25.8	24.78	0.10	22.97	0.10
1-147	638.9	192.8	3:33:43.45	-36:09:27.4	24.24	0.10	24.09	0.11
2-204	91.9	96.4	3:33:45.72	-36:09:07.2	23.77	0.10	22.00	0.10
2-659	123.7	230.4	3:33:46.38	-36:08:56.1	24.19	0.10	24.21	0.11
2-62	373.4	319.8	3:33:45.60	-36:08:31.4	22.95	0.10	21.74	0.11
2-333	511.4	324.3	3:33:44.88	-36:08:20.7	23.68	0.10	22.90	0.10
2-276	462.7	362.9	3:33:45.39	-36:08:21.9	23.42	0.10	23.21	0.10
2-467	255.3	505.2	3:33:47.39	-36:08:28.3	23.97	0.10	23.42	0.10
2-457	273.4	531.8	3:33:47.45	-36:08:25.2	24.09	0.10	23.18	0.10
2-288	244.6	553.5	3:33:47.74	-36:08:25.9	23.39	0.10	23.16	0.10
2-588	525.7	572.3	3:33:46.35	-36:08:03.5	24.31	0.10	23.86	0.10
2-319	522.2	601.6	3:33:46.55	-36:08:01.9	23.47	0.10	23.27	0.10
2-654	594.2	623.4	3:33:46.30	-36:07:55.0	24.31	0.10	24.09	0.10
2-138	596.1	643.8	3:33:46.42	-36:07:53.6	23.69	0.10	21.64	0.10
2-281	477.0	675.6	3:33:47.26	-36:08:00.5	23.67	0.10	22.72	0.10
3-73	338.3	81.9	3:33:47.59	-36:08:57.7	24.57	0.10	24.30	0.10
3-21	706.0	173.5	3:33:50.38	-36:08:40.9	23.95	0.10	22.94	0.10
3-4	453.7	201.5	3:33:48.95	-36:08:59.3	22.22	0.10	19.92	0.10
3-15	318.8	481.1	3:33:49.60	-36:09:29.2	23.70	0.10	23.50	0.10
3-72	304.7	499.6	3:33:49.61	-36:09:31.5	24.71	0.10	23.96	0.11
3-18	567.8	547.9	3:33:51.51	-36:09:18.1	23.69	0.10	23.63	0.10
3-64	481.1	556.0	3:33:51.02	-36:09:24.4	24.51	0.10	24.25	0.11
3-11	311.1	568.8	3:33:50.02	-36:09:36.3	23.68	0.10	22.27	0.10
3-37	446.6	580.6	3:33:50.93	-36:09:28.5	24.23	0.10	24.29	0.11
3-1	449.8	691.4	3:33:51.54	-36:09:36.6	20.95	0.10	19.60	0.10
3-2	719.9	715.5	3:33:53.36	-36:09:21.0	21.77	0.10	19.13	0.10
3-3	125.8	768.6	3:33:49.93	-36:10:03.4	21.91	0.10	19.52	0.10
4-52	355.4	94.0	3:33:46.85	-36:09:41.4	23.39	0.10	22.53	0.10

Table A1—Continued

Chip-ID	X	Y	RA (J2000)	Dec (J2000)	V	σ	I	σ
4-288	665.5	100.4	3:33:48.44	-36:10:05.5	24.39	0.10	24.47	0.11
4-322	208.0	106.1	3:33:45.99	-36:09:30.9	24.55	0.10	24.13	0.10
4-359	249.2	126.3	3:33:46.08	-36:09:35.4	24.69	0.10	24.62	0.11
4-173	304.7	140.1	3:33:46.29	-36:09:40.5	24.18	0.10	23.45	0.10
4-105	410.9	218.9	3:33:46.35	-36:09:53.7	23.69	0.10	23.72	0.11
4-140	329.5	233.4	3:33:45.83	-36:09:48.4	23.84	0.10	23.55	0.10
4-418	446.8	246.1	3:33:46.37	-36:09:58.1	24.74	0.10	24.74	0.11
4-214	370.6	274.1	3:33:45.79	-36:09:54.1	24.58	0.10	23.10	0.10
4-222	474.3	345.8	3:33:45.88	-36:10:06.6	24.23	0.10	23.86	0.10
4-116	454.0	369.4	3:33:45.63	-36:10:06.6	23.63	0.10	23.46	0.10
4-260	472.0	383.0	3:33:45.64	-36:10:08.8	24.28	0.10	23.93	0.10
4-43	221.8	394.2	3:33:44.25	-36:09:50.4	24.44	0.10	21.73	0.10
4-89	285.2	417.2	3:33:44.43	-36:09:56.7	24.50	0.10	22.32	0.10
4-242	331.2	532.3	3:33:43.95	-36:10:07.6	24.38	0.10	23.57	0.10
4-108	348.6	572.8	3:33:43.79	-36:10:11.5	23.92	0.10	22.89	0.10
4-221	616.4	752.3	3:33:44.07	-36:10:43.5	24.14	0.10	24.11	0.11

Table A2. Possible Variable Stars in NGC 1365

chip-id	x	y	V	V-I	P(days)
1-1298	113	735	26.12	1.22	28.6/29.1
1-1699	569	76	26.54	0.94	23.7/25.5
1-2514	458	618	26.37	0.44	36.4/41.4
1-1671	515	683	26.81	1.74	35.0
1-2931	524	511	27.08	1.14	17.2/18.2
1-2420	169	670	26.92	1.25	27.9/29.1
1-1085	763	184	26.19	0.92	16.8
1-1070	379	208	25.86	1.76	30.3
1-0066	262	322	27.60	0.88	36.3
2-1375	709	230	25.51	1.33	41.1
2-4325	549	491	26.57	1.09	21.0
2-4581	254	570	27.05	0.78	35.3
2-3175	760	268	26.49	0.78	24.2
2-5456	322	411	26.73	0.84	13.9
2-4065	392	555	26.56	0.72	22.1
2-6655	622	703	26.97	0.43	39.3
2-1969	679	490	25.83	1.00	24.0
3-2056	335	120	27.04	1.02	22.1/23.5
3-1696	495	444	26.91	1.18	29.0/33.3
3-776	465	575	26.36	1.05	24.0/29.0
3-1650	79	374	26.73	0.92	27.1/21.8
3-3233	502	408	27.16	1.11	19.8/36.3
3-946	78	173	26.37	0.36	12.3/24.5
3-2855	399	318	27.09	0.37	22.0
3-3747	468	446	27.31	-0.69	20.0
3-2658	478	465	26.88	0.43	13.8/23.0
4-1766	121	412	26.50	1.37	24.3
4-3052	515	551	26.56	0.65	14.2
4-1523	181	661	26.01	0.64	36.5
4-3271	132	670	26.79	0.66	39.0

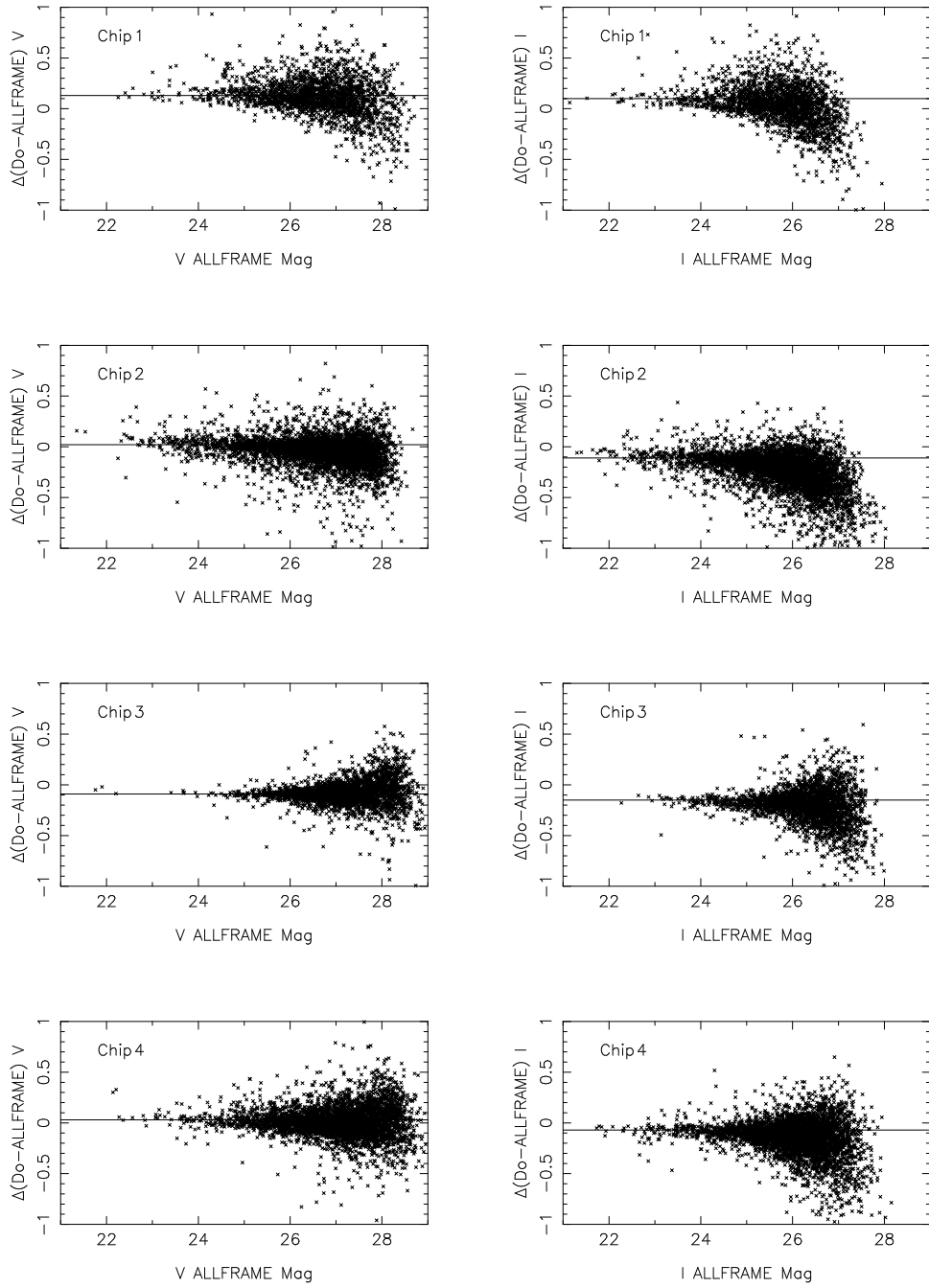


Fig. 2.— Comparison of the ALLFRAME and DoPHOT NGC 1365 photometry. Table 2 lists the mean differences between the photometry.

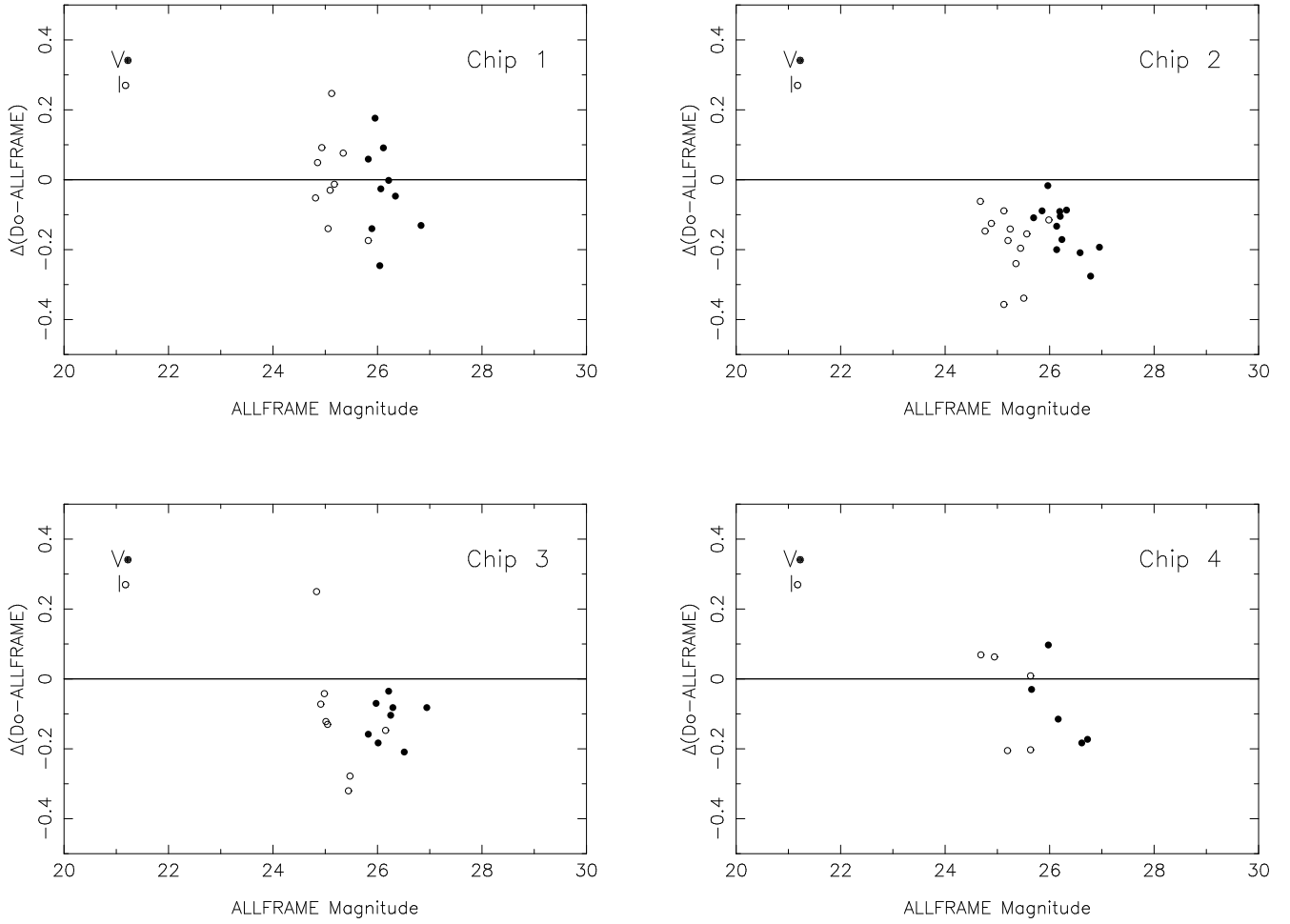


Fig. 3.— Comparison of the ALLFRAME and DoPHOT photometry for the 34 Cepheids in NGC 1365. The filled circles are the V comparisons and the open circles are the I comparisons. Table 2 lists the mean differences between the ALLFRAME and DoPHOT photometry.

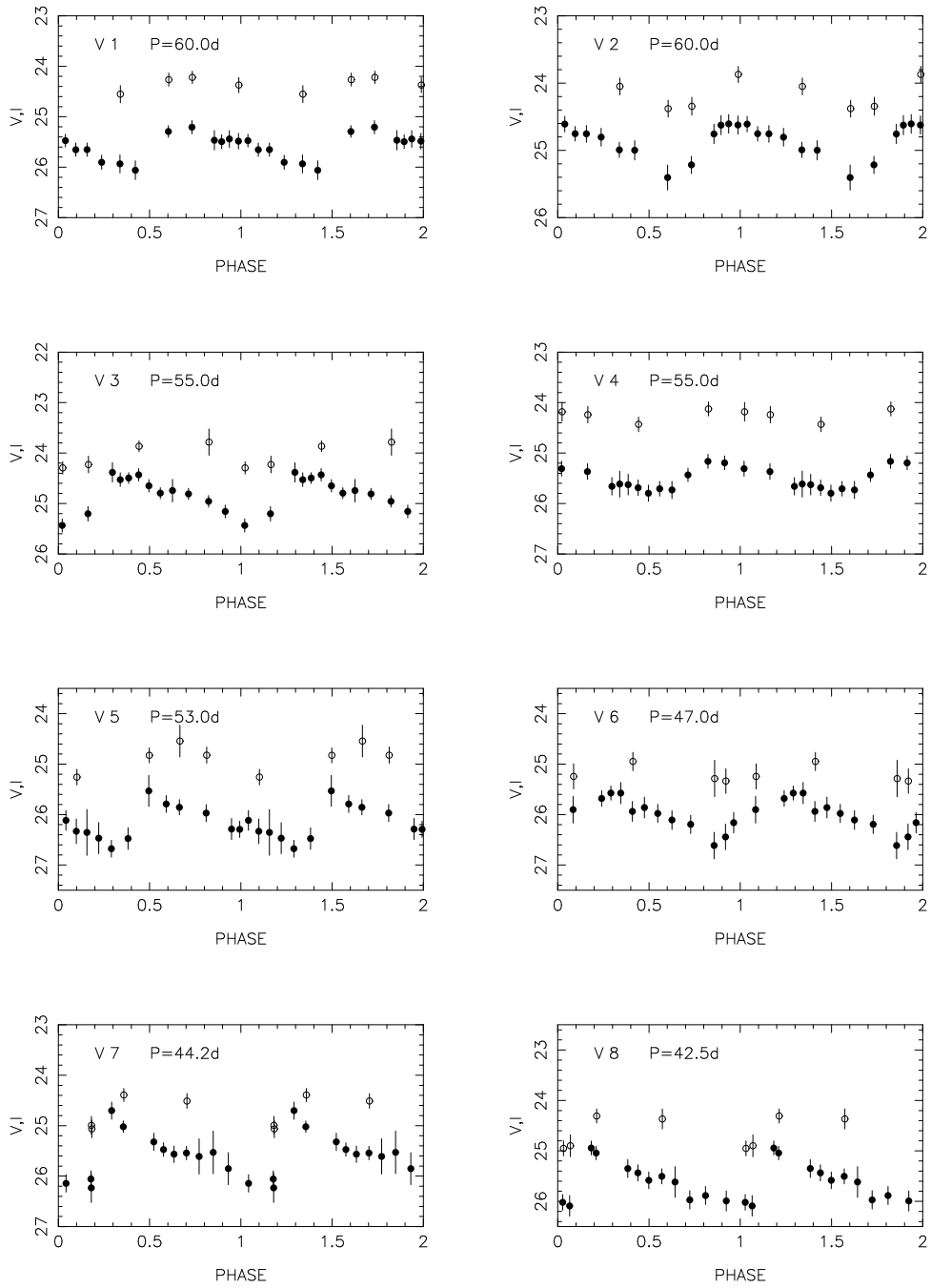


Fig. 6.— *V* and *I* light curves are presented for the 52 Cepheids in NGC 1365. The data are repeated over a second cycle for clarity. *V* data are filled circles. *I* data are open circles.

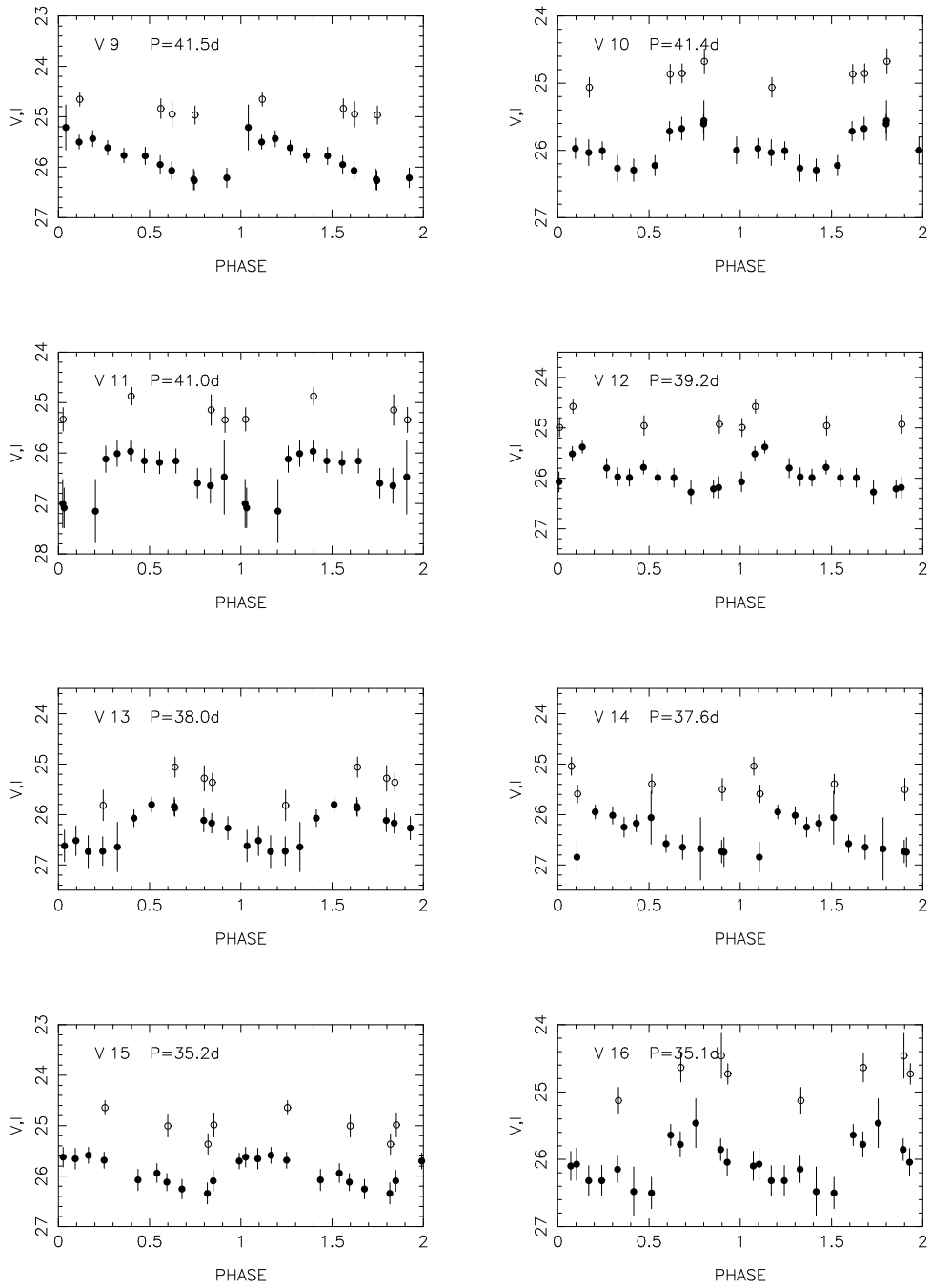


Fig. 6.— *V* and *I* light curves are presented for the 52 Cepheids in NGC 1365. The data are repeated over a second cycle for clarity. *V* data are filled circles. *I* data are open circles.

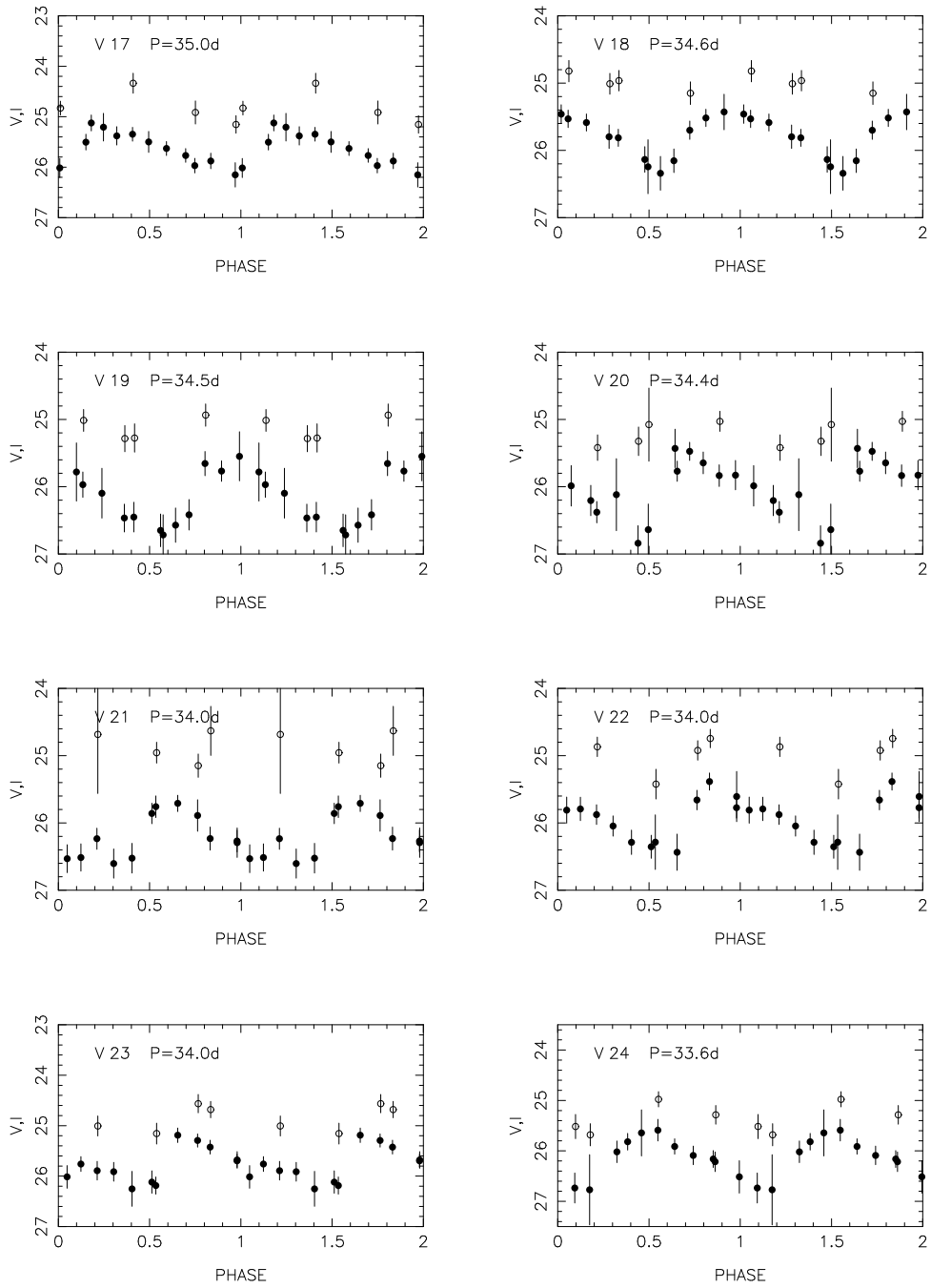


Fig. 6.— *V* and *I* light curves are presented for the 52 Cepheids in NGC 1365. The data are repeated over a second cycle for clarity. *V* data are filled circles. *I* data are open circles.

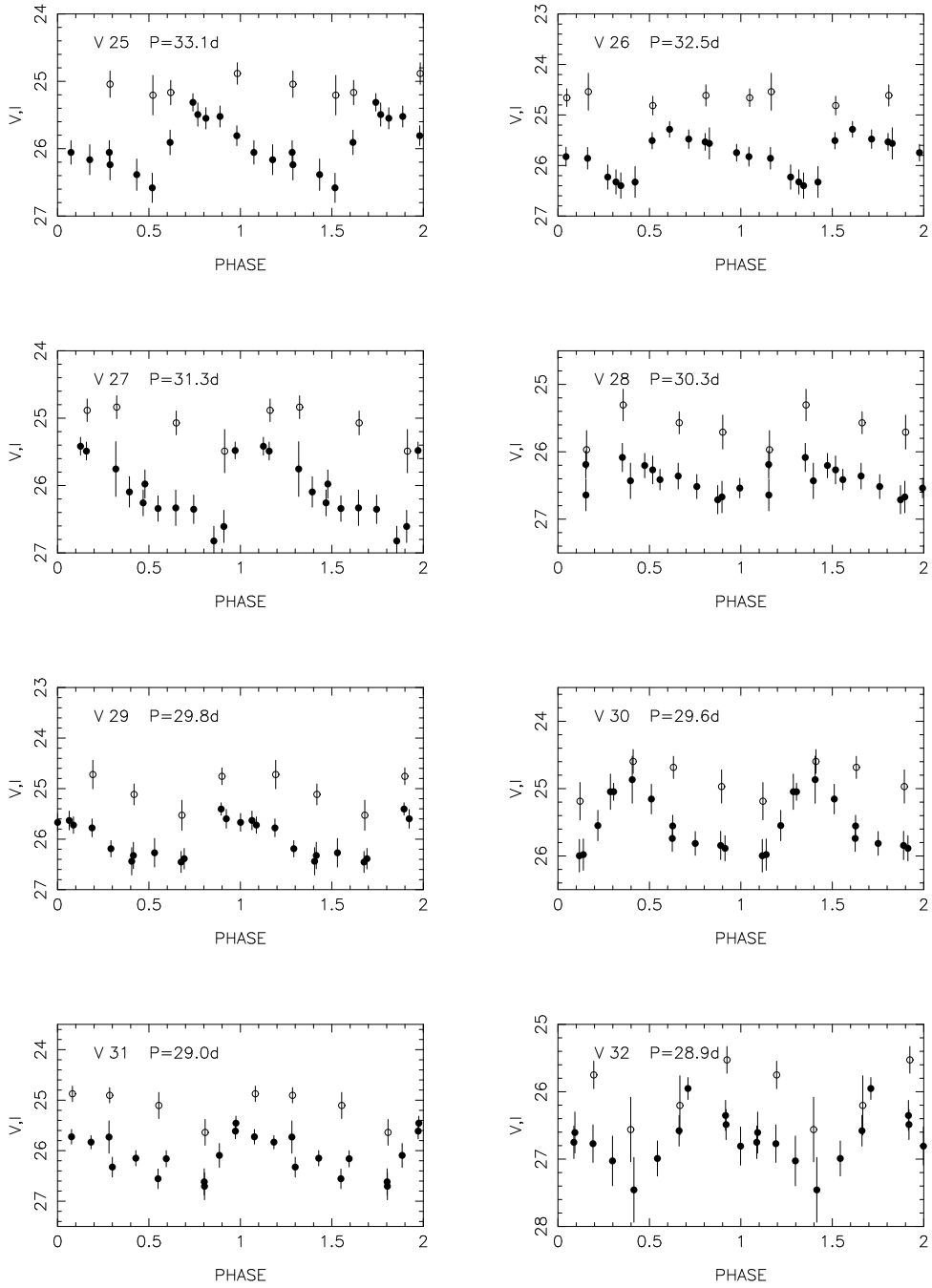


Fig. 6.— *V* and *I* light curves are presented for the 52 Cepheids in NGC 1365. The data are repeated over a second cycle for clarity. *V* data are filled circles. *I* data are open circles.

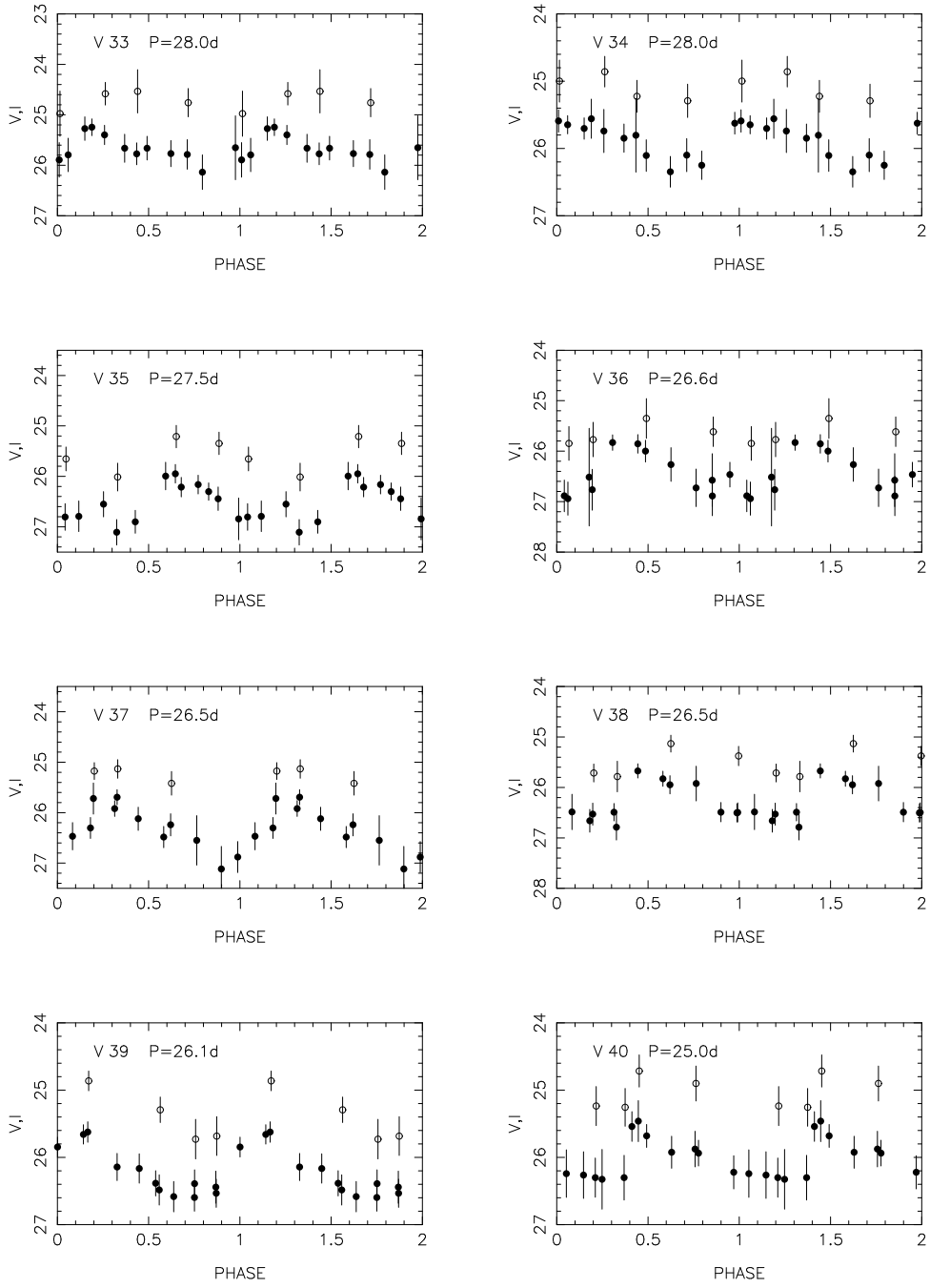


Fig. 6.— *V* and *I* light curves are presented for the 52 Cepheids in NGC 1365. The data are repeated over a second cycle for clarity. *V* data are filled circles. *I* data are open circles.

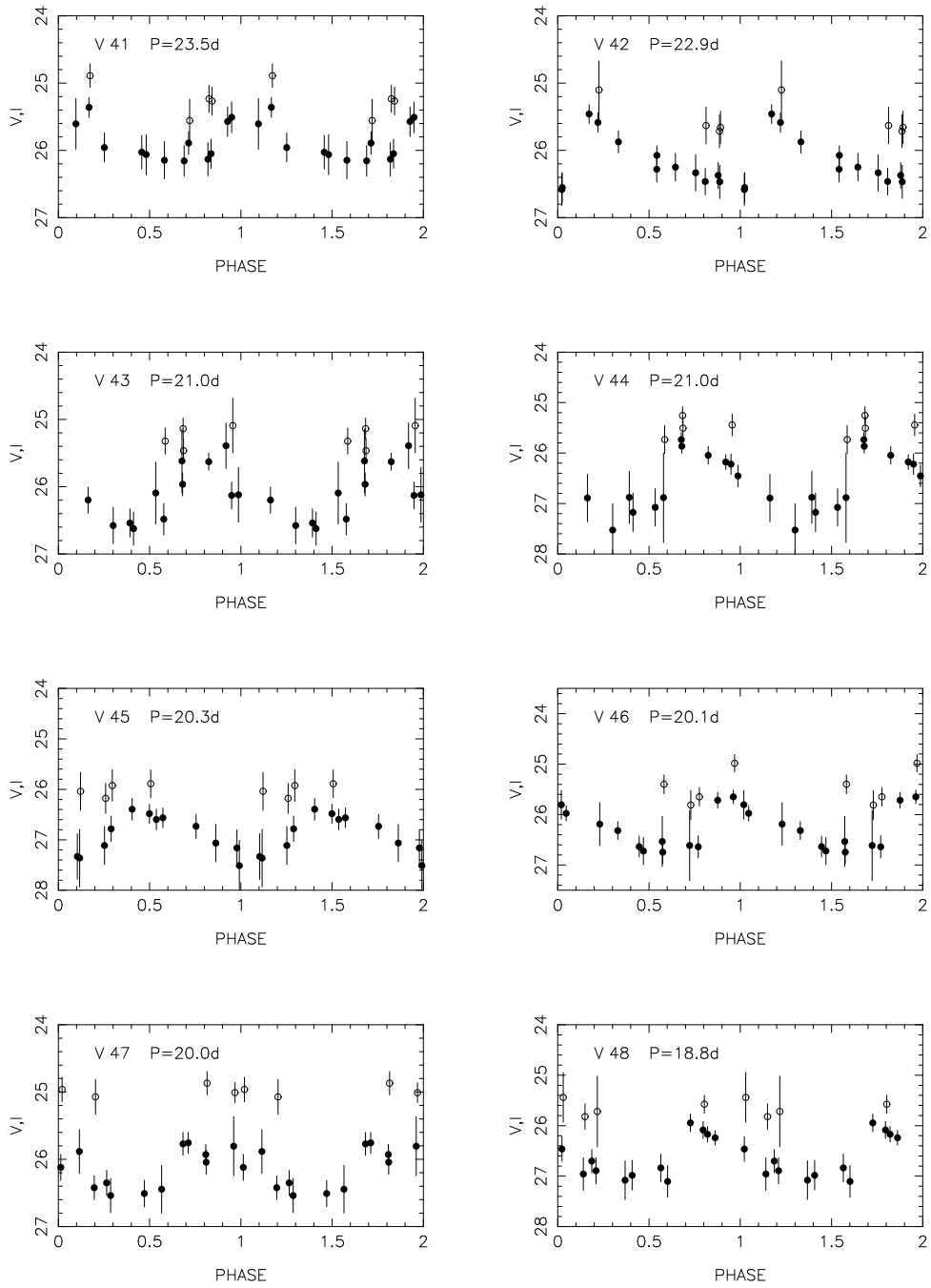


Fig. 6.— V and I light curves are presented for the 52 Cepheids in NGC 1365. The data are repeated over a second cycle for clarity. V data are filled circles. I data are open circles.

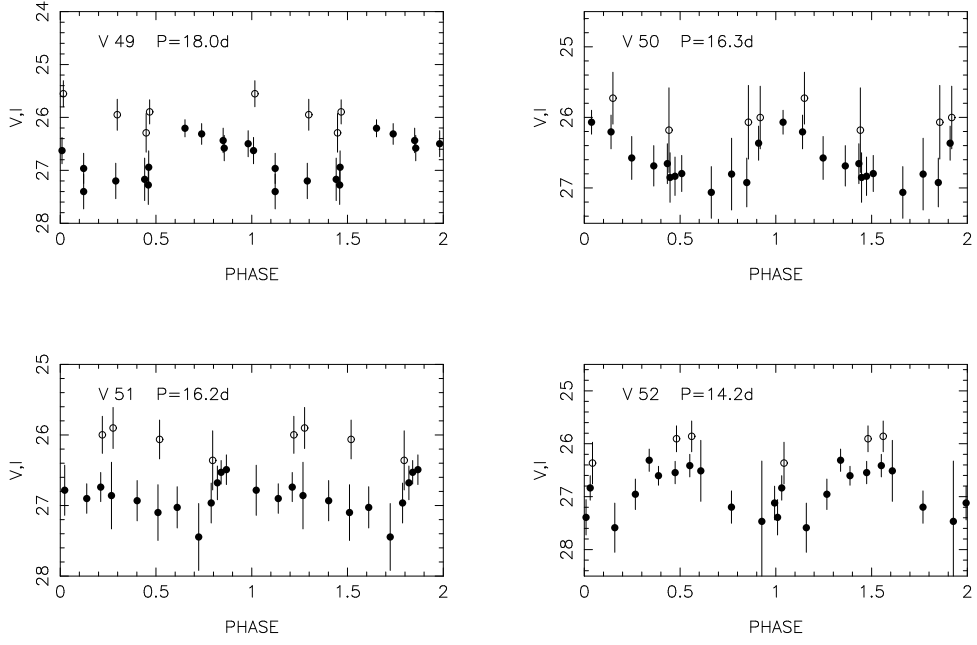


Fig. 6.— V and I light curves are presented for the 52 Cepheids in NGC 1365. The data are repeated over a second cycle for clarity. V data are filled circles. I data are open circles.

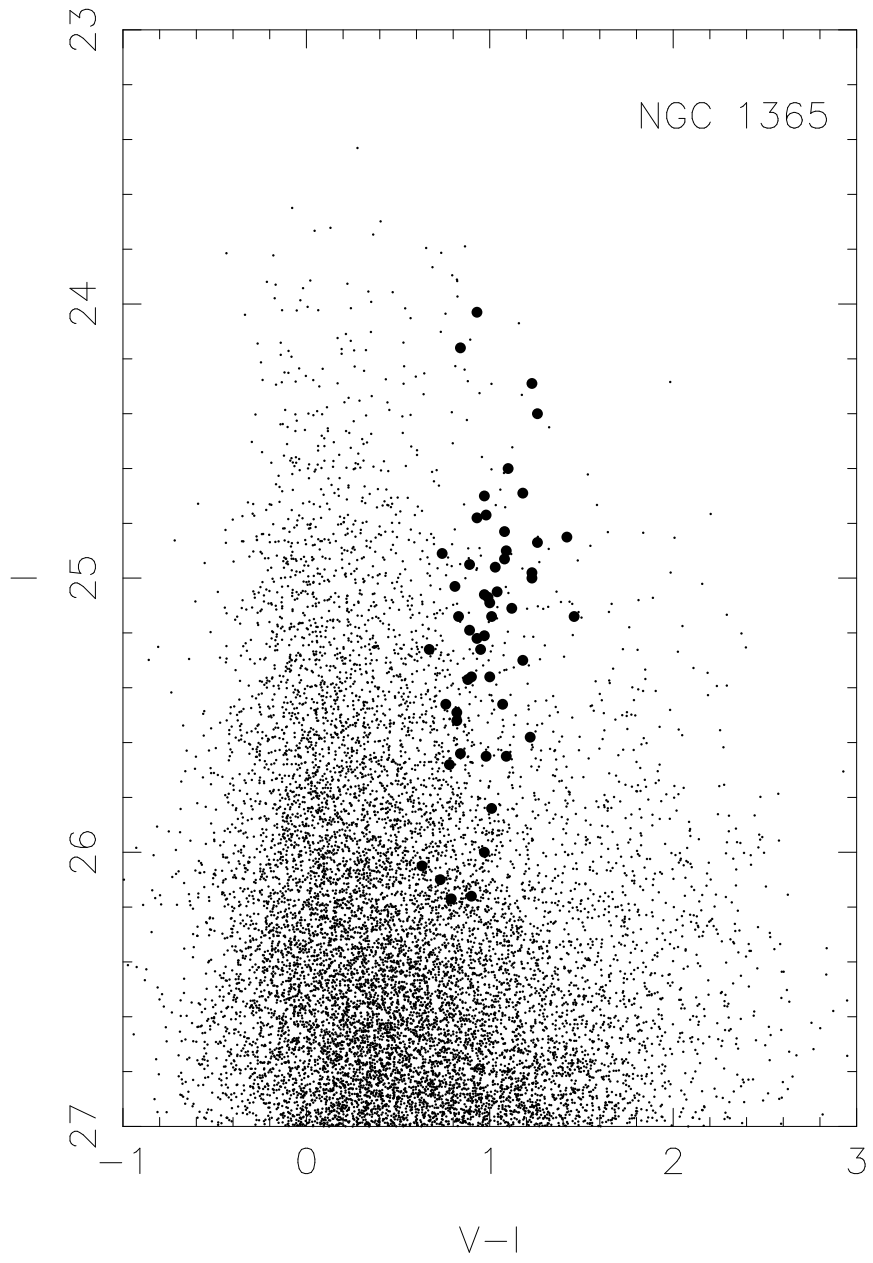


Fig. 7.— Color-magnitude diagram for the HST field of NGC1365. Cepheids are indicated by the large filled circles.

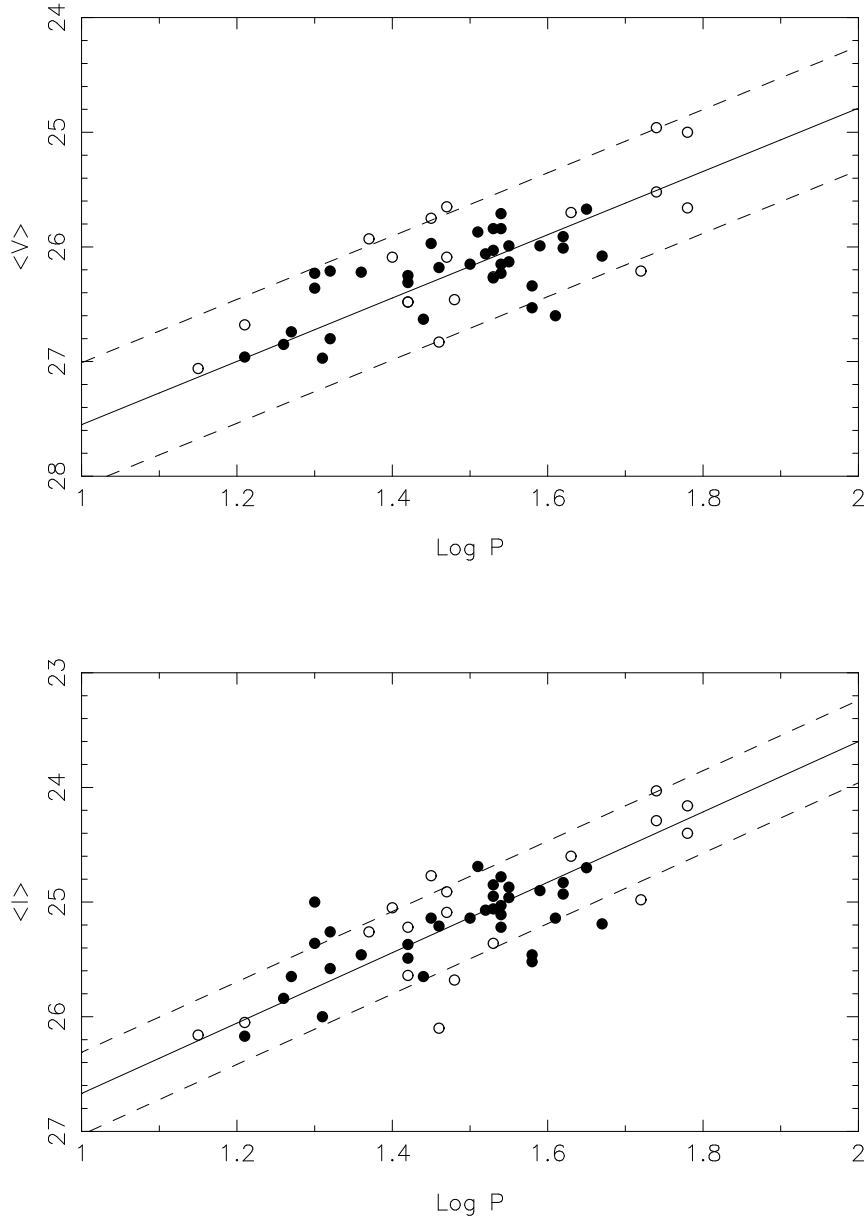


Fig. 8.— ALLFRAME V and I period-luminosity relations for the Cepheids in NGC 1365. The filled circles are those Cepheids used to determine the distance to NGC 1365. The open circles are the rest of the Cepheids. The solid line is the best fit to the NGC 1365 data. The dotted lines indicate the expected scatter due to the intrinsic width of the Cepheid instability strip.

This figure "p33.gif" is available in "gif" format from:

<http://arxiv.org/ps/astro-ph/9806017v1>

This figure "p36.gif" is available in "gif" format from:

<http://arxiv.org/ps/astro-ph/9806017v1>

This figure "p37.gif" is available in "gif" format from:

<http://arxiv.org/ps/astro-ph/9806017v1>

This figure "p38.gif" is available in "gif" format from:

<http://arxiv.org/ps/astro-ph/9806017v1>

This figure "p39.gif" is available in "gif" format from:

<http://arxiv.org/ps/astro-ph/9806017v1>